Journal of Wind Engineering & Industrial Aerodynamics 189 (2019) 71–90

Contents lists available at ScienceDirect

Journal of Wind Engineering & Industrial Aerodynamics

journal homepage: www.elsevier.com/locate/jweia

Directional decomposition and properties of thunderstorm outflows

Shi Zhang [a,b,d,*], Giovanni Solari [a], Massimiliano Burlando [a], Qingshan Yang [c,d]

[a] Department of Civil, Chemical and Environmental Engineering, University of Genoa, Italy
[b] School of Civil Engineering, Beijing Jiaotong University, China
[c] School of Civil Engineering, Chongqing University, China
[d] Beijing's Key Laboratory of Structural Wind Engineering and Urban Wind Environment, China

ARTICLE INFO

Keywords:
Decomposition rule
Monitoring network
Thunderstorm outflow
Wind dataset
Wind properties

ABSTRACT

Thunderstorm outflows are usually analysed by decomposing their horizontal velocity into a slowly-varying mean part and a residual fluctuation; in this framework the wind direction is often examined qualitatively but disregarded quantitatively. This is incoherent with the traditional analysis of synoptic wind speeds, where the mean velocity and direction are first determined, then the fluctuations are decomposed in terms of longitudinal and lateral turbulence components. Aiming to overcome these shortcomings, a novel directional decomposition strategy is formulated here, which makes the study of thunderstorm outflows and synoptic winds fully coherent. The results provided by the classic and novel decomposition rules are first compared and elucidated with reference to a couple of real thunderstorm and synoptic wind velocity records. Later on, they are applied to a broad class of thunderstorm outflow records whose statistical properties are investigated. The novel approach is strategic to carry out directional analyses of the dynamic behaviour of structures in terms of alongwind and crosswind response.

1. Introduction

The constitutive deed of wind engineering is usually identified with a paper in which Davenport (1961) embedded the fundamentals of meteorology, micrometeorology, climatology, aerodynamics and structural dynamics into a homogeneous framework of the wind loading of structures now recognised as "Davenport chain". In such a context, the wind model conceived by Davenport as the first ring of his chain refers to an extra-tropical cyclone at the synoptic scale. In addition, thanks to the principles introduced by Van der Hoven (1957), the wind speed is expressed as the sum of a mean part, related to the macro-meteorological peak, and of a residual fluctuation of turbulent nature, corresponding to the micro-meteorological peak.

Accordingly, within time intervals belonging to the spectral gap that separates the two peaks, namely in the range between 10 min and 1 h, the mean wind velocity and its direction are assumed as constant whereas the turbulent fluctuation is dealt with as a stationary Gaussian random process. In addition, turbulence is decomposed in terms of a longitudinal component, aligned with the mean wind velocity, a lateral component, orthogonal to the mean wind velocity and parallel to the ground, and a vertical component. Among many other advantages, this model facilitates the classical analysis of the structural behaviour in terms of its alongwind and crosswind (lateral and/or vertical) response (e.g. Piccardo and Solari, 2000).

With the passing of time wind engineering has dedicated more and more interest to the topic of mixed climate (Gomes and Vickery, 1977/1978), namely the study of climatic conditions in which the wind can manifest itself in multiple forms such as extra-tropical and tropical cyclones, monsoons, tornadoes, thunderstorm downbursts and downslope winds. For each of these phenomena, ever more detailed models have been developed. In this framework, great attention has been dedicated to downbursts (Fig. 1) and to their actions and effects on structures (Letchford et al., 2002; Solari, 2014). They are transient events at the mesoscale that frequently cause wind speeds greater than those due to synoptic cyclones (Fujita, 1985; Lombardo et al., 2014; Zhang et al., 2018b). The scale of these phenomena and their non-stationary character make the application of the principles enunciated by Van der Hoven (1957) and the separation of the wind speed into a mean value and a residual fluctuation quite problematic.

The first analytical models of the thunderstorm wind velocity applied fluid dynamic laws to stationary flows in order to obtain simple analytical expressions, independent of time, of the vertical and radial components of the wind velocity. This led to the formulation of the impinging wall jet (Oseguera and Bowles, 1988; Vicroy, 1991) and vortex ring (Zhu and

* Corresponding author. Department of Civil, Chemical and Environmental Engineering, University of Genoa, Italy.
E-mail address: 10231097@bjtu.edu.cn (S. Zhang).

https://doi.org/10.1016/j.jweia.2019.03.014
Received 15 November 2018; Received in revised form 7 March 2019; Accepted 10 March 2019
Available online 31 March 2019

Etkin, 1985; Ivan, 1986; Schultz, 1990; Vicroy, 1992) models. Holmes and Oliver (2000) applied the impinging wall jet model by expressing the radial component of the wind velocity as a function of the distance from the jet axis and of the time; they also expressed the horizontal velocity as the vector summation of the stationary radial outflow velocity and of the translational velocity of the thunderstorm cell.

A turning point occurred when Choi and Hidayat (2002) expressed the horizontal component of the wind velocity as the sum of its slowly-varying mean part, averaged on a suitable moving average period, plus a residual fluctuation. This approach was developed later by Chen and Letchford (2004a, 2004b, 2007), Chay et al. (2006), Ponte and Riera (2007, 2010), Holmes et al. (2008), and Huang et al. (2015), who expressed the slowly-varying mean wind velocity as the product of a function depending on space, provided by the previous time-independent analytical models (Oseguera and Bowles, 1988; Zhu and Etkin, 1985; Ivan, 1986; Vicroy, 1992), by a slowly-varying function of time. The fluctuation, dealt with as non-stationary, was given by the product of its slowly-varying standard deviation by a random stationary Gaussian process with zero mean and unit standard deviation.

A relevant part of this research activity focused on how to separate the slowly-varying mean wind velocity from the residual fluctuation without availing of a clear spectral gap. In this framework, the slowly-varying mean wind velocity has been extracted by means of wavelets, empirical mode decomposition and kernel regression (Chen and Letchford, 2007; McCullough et al., 2014; Su et al., 2015) or, more easily, by a moving average filter (Choi and Hidayat, 2002), around which a huge discussion occurred on the most suitable choice of the moving average period (Choi and Hidayat, 2002; Chen and Letchford, 2005, 2006; Holmes et al., 2008; Orwig and Schroeder, 2007; Riera and Ponte, 2012; Lombardo et al., 2014; Solari et al., 2015a).

Very strangely, instead, nobody discussed, at authors' knowledge, a couple of relevant shortcomings involved by the classical decomposition rule rapidly become a sort of axiom. First of all, even if many papers provided a clear discussion on the sudden and large changes frequently exhibited by the wind direction in the course of thunderstorm outflows (Choi, 2000; Holmes et al., 2008; De Gaetano et al., 2014), the wind direction remained outside the decomposition rule from a quantitative viewpoint. In addition, in a totally different way from the classic analysis of synoptic winds, no decomposition was applied to separate the longitudinal turbulence from the lateral one. These aspects created at least three main shortcomings.

First, they caused a deep difference between the study of synoptic and thunderstorm wind speeds, making quite questionable any comparison between the properties of these two phenomena. Second, they oriented the literature on the dynamic response of structures to thunderstorm outflows towards the implicit assumption that the response occurred in the alongwind direction (Choi and Hidayat, 2002; Chen and Letchford, 2004b; Chen, 2008; Kwon and Kareem, 2009; Huang et al., 2013; Solari et al., 2015b; Solari, 2016; Solari et al., 2017; Solari and De Gaetano, 2018; Peng et al., 2018), precluding any chance to separate the alongwind response from the crosswind one, as it is classical, and, even more, to take into account the changes of the angle of attack jointly due to the turbulent fluctuations and to the rapid changes of the wind direction. Third, they did not provide any element to robustly take into account the change of direction in at least two relevant problems: the increase of the speed in thunderstorm outflows due to downburst translation and background flow (Miguel et al., 2018) and the reconstruction of these events through evolutionary models based on measurements and simulations (Abd-Elaal et al., 2013). To overcome these shortcomings, a novel directional decomposition strategy of the wind speed is herein formulated that opens the doors to a robust comparison and parallel analyses of thunderstorm outflows and synoptic winds in terms of wind speed, wind loading and structural response. It also makes possible an appropriate treatment of all the problems in which the change of direction plays a significant role. This strategy is applied, in the framework of the ERC (European Research Council) Project THUNDERR (www.thunderr.eu), to the anemometric records detected during two previous European Projects, "Wind and Ports" (Solari et al., 2012) and "Wind, Ports and Sea" (Repetto et al., 2018).

Section 2 illustrates the main properties of the wind monitoring network and the dataset of thunderstorm outflows used for this study. Section 3 and 4 describe the classical decomposition rules commonly applied to synoptic and thunderstorm outflows, respectively, elucidating their properties through inspecting two typical recordings. Section 5 introduces the new directional decomposition rule and compares it with the classical ones using as a reference the typical recordings analysed in the previous two sections. Section 6 analyses an extensive set of thunderstorm outflow recordings using both the classical and the novel strategy in a statistical environment. Section 7 points out the main conclusions and draws some prospects for future research.

2. Wind monitoring network and thunderstorm outflow dataset

"Wind and Ports" (WP) (Solari et al., 2012) and "Wind, Ports and Sea" (WPS) (Repetto et al., 2018) were two projects financed by the European Cross-border program "Italy–France Maritime 2007–2013" in order to establish the safe and operational management of the main commercial seaports of the High Tyrrhenian areas during intense wind events.

One of the objectives of the WP and WPS Projects was the realization of a wind monitoring network in the port areas of Genoa, Livorno, Savona and Vado Ligure, La Spezia, Bastia and L'Île-Rousse. During the WP Project, 23 ultra-sonic anemometers were installed. Later on, during the WPS Project, the network was enlarged by means of 3 LiDAR (Light

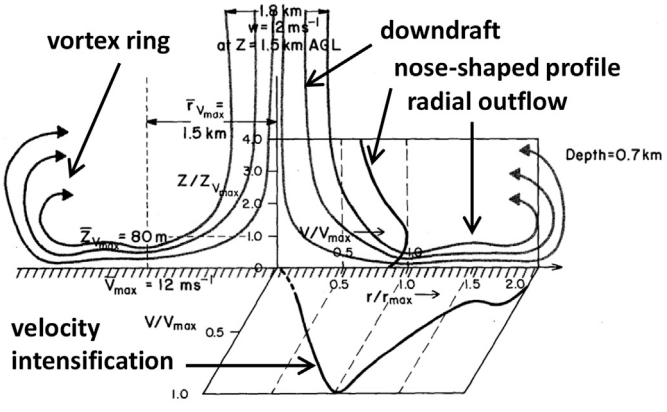

Fig. 1. Thunderstorm downburst: structure of the outflow at maximum intensity and schematic view of its main features (after Hjelmfelt, 1988).

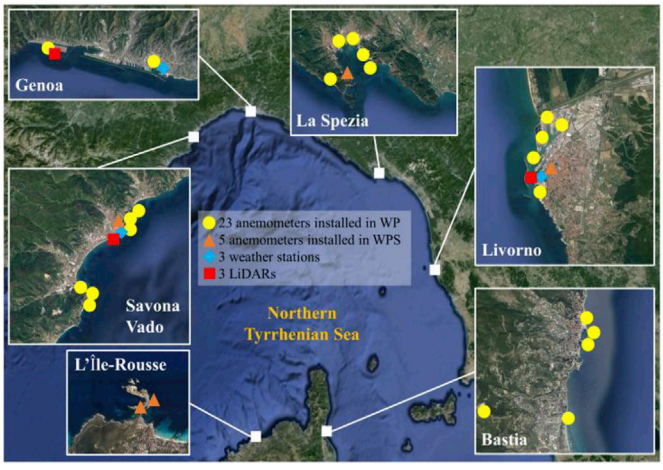

Fig. 2. WP and WPS wind monitoring network (Repetto et al., 2018).

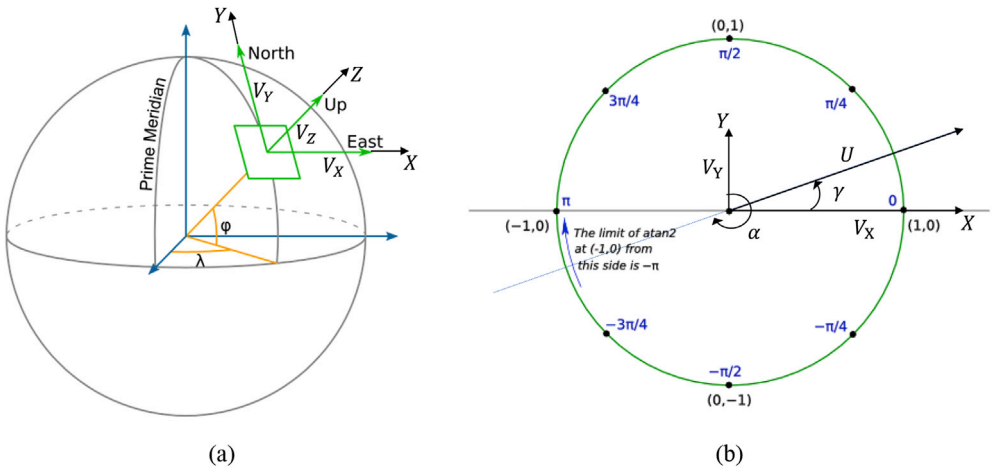

(a) (b)

Fig. 3. (a) space coordinate system adopted for the anemometric measurements; (b) decomposition of the horizontal component of the wind speed and atan2 rationale.

Detection And Ranging) wind profilers and 3 weather stations, each one including an additional ultra-sonic anemometer, a barometer, a thermometer and a hygrometer. Moreover, 5 ultra-sonic anemometers were mounted in the port areas of Savona, La Spezia, Livorno and L'Île Rousse. Fig. 2 shows the current network composition. Beside its original institutional purpose, it provides a unique opportunity to detect high resolution thunderstorm records and study their dominant properties (Solari, 2014).

The position of the anemometers was chosen in order to cover homogeneously the port areas and register undisturbed wind velocity histories. The instruments were generally mounted on high-rise towers or on antenna masts at the top of buildings, paying attention to avoid local effects that could contaminate the measurements. The height h of the anemometers varies from 10 m to 84 m above the ground level (AGL). Their sampling rate is 10 Hz, with the exception of the sensors installed in the Ports of Bastia and L'Île-Rousse whose sampling rate is 2 Hz.

The anemometric data, measured with a precision of 0.01 m/s, are stored in terms of their components (V_X, V_Y) for bi-axial anemometers or (V_X, V_Y, V_Z) for three-axial anemometers, according to the geophysical coordinate system (Fig. 3a), where V_X is directed from West to East, V_Y from South to North, and V_Z is vertical and positive upwards.

Focusing on the horizontal components of the wind speed (V_X, V_Y), they can also be expressed in terms of the resultant wind speed U and the wind direction α (Fig. 3b):

$$\begin{aligned} U(t) &= \sqrt{V_X^2(t) + V_Y^2(t)} \\ \alpha(t) &= 270 - \text{atan2}(V_Y(t)/V_X(t)) \\ \gamma\ (t) &= 270 - \alpha(t) \end{aligned} \tag{1}$$

where $\alpha \in [0:360]$ is a clockwise directional angle, computed from Y (North), referred to the geographical notation commonly used in atmospheric sciences, $\gamma \in [0:360]$ is an anti-clockwise directional angle, computed from X (East), frequently used in wind engineering.

A set of local servers placed in each Port Authority headquarter receives the data acquired by the anemometers in their own port area and automatically transfers the raw data stored in 10-min long files to a central server at the Department of Civil, Chemical and Environmental Engineering (DICCA) of the University of Genova.

Coherently with the modern trends for mixed wind climates (Gomes and Vickery, 1977/1978; Kasperski, 2002; Lombardo et al., 2009; Solari, 2014), Solari et al. (2015a) analysed the data provided by 9 ultra-sonic anemometers in the period 2011–2012 to extract and separate sub-datasets collecting intense wind events related to different phenomena, i.e. extra-tropical cyclones, thunderstorm outflows and intermediate events. According to the criteria described by De Gaetano et al. (2014), this analysis led to extract 93 strongly non-stationary records that were traced back to convective conditions and thunderstorm outflows.

Zhang et al. (2018a) extended this study to the data recorded by 14 ultra-sonic anemometers, including the 9 ones previously studied, in the period 2010–2016. This new analysis led to the extraction of 277 strongly non-stationary records that, likewise and better than the previous ones, were initially traced back to convective conditions and thunderstorm outflows. In this regard, such records were separated into 3 families depending on whether the presence of an evident peak was clear over 10-min, 1-h or 10-h periods; this aspect reflects on the passage duration of the gust front.

Subsequent investigations aiming to interpret the weather scenarios in which transient events occur (Burlando et al., 2017, 2018) clarified that the records whose peak is clear only over 10-h periods, initially misclassified as potential thunderstorms, should be more likely catalogued as rapidly evolving extra-tropical cyclones. In this paper, only the 141 records related to the 10-min family are used (Table 1) to elucidate the new directional decomposition rule and compare the properties of thunderstorm outflows evaluated by the new rule and the classical one (Zhang et al., 2018a).

A dominant property of the above dataset and of the following estimates is the large number of thunderstorm records detected and gathered in order to carry out statistical analyses of their main parameters. Approaching this issue with the same spirit usually adopted for synoptic wind speeds (Solari and Piccardo, 2001), this is possible by reducing the extraction threshold (here, thunderstorm outflows with peak wind speed

Table 1
Main properties of the ultrasonic anemometers examined and number of thunderstorm records (NTR) selected (Zhang et al., 2018a).

Port	Anem. No.	h (m)	Type	Period of analysis	NTR
Genoa	1	61.4	bi-	2011.03.30–2013.04.01	5
	2	13.3	axial	2010.10.12–2015.05.31	11
Livorno	1	20	tri-	2010.10.01–2015.12.12	19
	2	20	axial	2010.10.01–2015.12.12	8
	3	20		2010.10.01–2015.03.21	15
	4	20		2010.10.01–2015.12.12	18
	5	75		2010.10.01–2014.08.25	6
Savona and Vado	1	33.2	tri-	2014.12.01–2016.01.31	3
	2	12.5	axial	2014.12.01–2016.01.31	1
	3	28		2014.12.01–2016.01.31	6
	4	32.7		2014.12.01–2016.01.31	7
	5	44.6		2014.12.01–2016.01.31	2
La Spezia	2	13	bi-	2010.10.29–2015.12.31	12
	3	10	axial	2011.02.05–2015.12.18	28
All ports	14	–		–	141

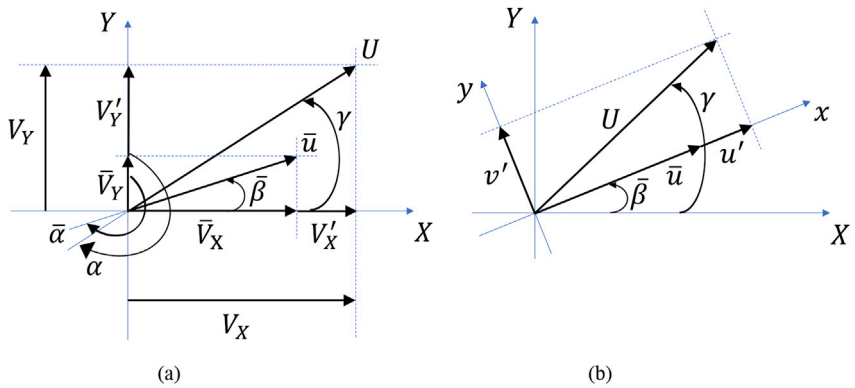

Fig. 4. Classical decomposition of the wind speed for synoptic phenomena.

above 15 m/s) and processing data through suitable non-dimensional quantities. The alternative, not used herein, is increasing the extraction threshold and studying intense thunderstorm scenarios without any probabilistic interpretation. On passing the time and increasing the number of records, it will be possible to process thunderstorm outflows in a probabilistic environment that takes the wind speed into account.

In the meanwhile, based on 7 years of recordings, the highest peak wind speed of the measured thunderstorm outflows reached 34 m/s, with a return period around 10 years (Zhang et al., 2018b). The wind speed of transient events exceeds the one of synoptic winds for return periods above 1–5 years.

3. Classical decomposition for synoptic winds

Adopting the classical decomposition rule for synoptic phenomena, the two horizontal components of the wind speed are usually expressed as (Fig. 4a):

$$\begin{aligned} V_X(t) &= \overline{V}_X + V_X^{'}(t) \\ V_Y(t) &= \overline{V}_Y + V_Y^{'}(t) \end{aligned} \tag{2}$$

where $t \in [0,\ \Delta T]$ is the time, being herein $\Delta T = 10$ min, $\overline{V}_X$ and $\overline{V}_Y$ are the mean values of V_X and V_Y over the time interval ΔT, $V^{'}_X$ and $V^{'}_Y$ are the residual turbulent fluctuations of V_X and V_Y with respect to $\overline{V}_X$ and $\overline{V}_Y$.

Based upon Eq. (2) the mean wind velocity and its direction are given by (Fig. 4a):

$$\begin{aligned} \overline{u} &= \sqrt{\overline{V}_X^2 + \overline{V}_Y^2} \\ \overline{\alpha} &= 270 - \mathrm{atan2}\left(\overline{V}_Y / \overline{V}_X\right) \\ \overline{\beta} &= 270 - \overline{\alpha} \end{aligned} \tag{3}$$

where $\overline{\alpha}, \overline{\beta} \in [0 : 360]$. Accordingly, $V^{'}_X$ and $V^{'}_Y$ are projected onto a new Cartesian reference system (x, y), where the x-axis coincides with the direction of the mean wind velocity $\overline{u}$ and is rotated $\overline{\beta}$ with respect to the fixed X-axis. Thus (Fig. 4b):

$$\begin{aligned} u^{'}(t) &= V_X^{'}(t)\cos\overline{\beta} + V_Y^{'}(t)\sin\overline{\beta} \\ v^{'}(t) &= -V_X^{'}(t)\sin\overline{\beta} + V_Y^{'}(t)\cos\overline{\beta} \end{aligned} \tag{4}$$

where $u^{'}$ and $v^{'}$ are the longitudinal and lateral turbulent components. Eq. (4) can also be re-written as:

$$\begin{aligned} u^{'}(t) &= \sigma_u \tilde{u}^{'}(t) \\ v^{'}(t) &= \sigma_v \tilde{v}^{'}(t) \end{aligned} \tag{5}$$

where σ_u and σ_v are the standard deviations of $u^{'}$ and $v^{'}$ over ΔT, $\tilde{u}^{'}$ and $\tilde{v}^{'}$ are the reduced longitudinal and lateral turbulence components. The latter terms are usually modelled as un-correlated stationary Gaussian random processes with zero mean and unit standard deviation (Solari and Piccardo, 2001).

Thanks to Eqs. (3)–(5) the longitudinal and lateral components of the wind velocity can be expressed as:

$$\begin{aligned} u(t) &= \overline{u} + u^{'}(t) = \overline{u}\left[1 + I_u \tilde{u}^{'}(t)\right] \\ v(t) &= v^{'}(t) = \overline{u} I_v \tilde{v}^{'}(t) \end{aligned} \tag{6}$$

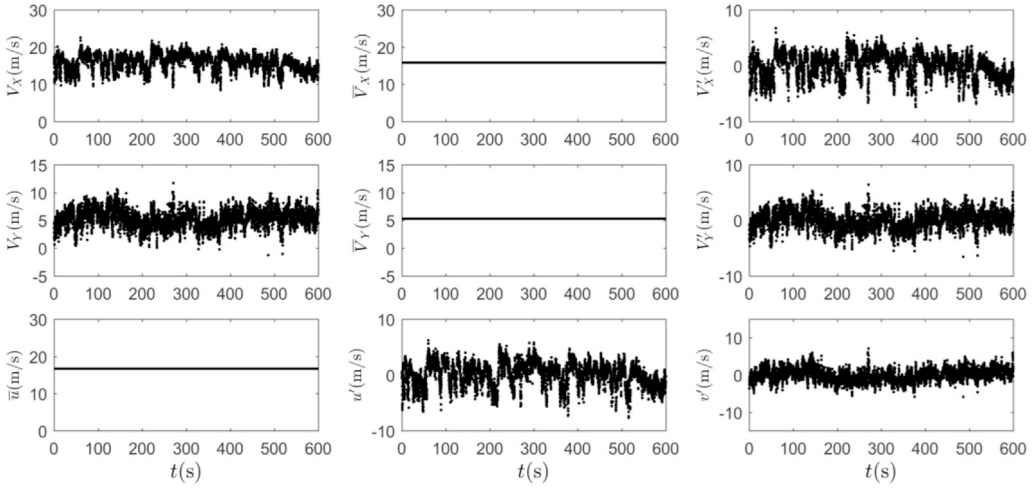

Fig. 5. Application of Eqs. (2) to (4) to a typical synoptic extra-tropical cyclone.

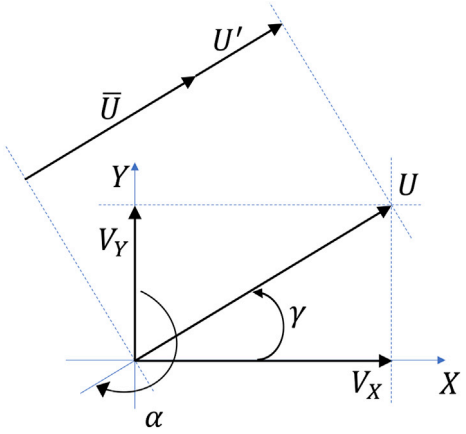

Fig. 6. Classical decomposition of the wind speed for thunderstorm outflows.

where I_u and I_v are the longitudinal and lateral turbulence intensities:

$$I_u = \sigma_u/\overline{u}$$
$$I_v = \sigma_v/\overline{u} \tag{7}$$

Literature is usual to assign $I_v/I_u = 0.75$ (Solari and Piccardo, 2001). Finally, the gust factor is expressed as:

$$G_u = \widehat{u}/\overline{u} \tag{8}$$

where $\widehat{u}$ is the peak longitudinal velocity defined here as the maximum longitudinal wind velocity averaged over a $\tau = 1$-s period.

Fig. 5 shows the application of Eqs. (2)–(4) to the wind velocity of a synoptic extra-tropical cyclone recorded on July 8, 2014 by the anemometer 1 of the Port of Livorno; both the velocity components V_X and V_Y exhibit a typical stationary trend. In this case, $\overline{u} = 16.71$ m/s, $\overline{\alpha} = 251.51°$, $I_u = 0.13$, $I_v = 0.10 = 0.76 I_u$, $\rho_{uv} = -0.11$, ρ_{uv} being the cross-correlation coefficient of u' and v'. In addition, the latter quantities have skewness values $\gamma_u = -0.40$ and $\gamma_v = 0.16$ whereas their kurtosis values are $\kappa_u = 2.65$ and $\kappa_v = 2.99$. All these values are coherent with those classically reported by the literature with regard to synoptic phenomena.

It is worth noting, however, that having determined the mean wind velocity over ΔT, the residual fluctuations contain harmonic contents both in the low-frequency range (slowly-varying long waves) and in the high-frequency range (rapidly-varying short oscillations).

4. Classical decomposition for thunderstorm outflows

Let us consider the horizontal components of the wind velocity U and its direction γ or α as defined by Eq. (1) and Fig. 3b. It is worth noticing that most papers dealing with thunderstorm outflows provide diagrams of both the U and γ or α time-histories (Choi, 2000; Holmes et al., 2008; De Gaetano et al., 2014). However, while the velocity is later analysed in detail as described hereinafter, the direction is considered only on a qualitative level. Under this point of view, as an example, most research carried out on the dynamic response of structures to thunderstorm outflows (Choi and Hidayat, 2002; Chen and Letchford, 2004b; Chen, 2008; Kwon and Kareem, 2009; Solari et al., 2015b; Solari, 2016; Solari et al., 2017; Solari and De Gaetano, 2018) implicitly deals with a sort of alongwind response, disregarding the fact that the wind direction often varies rapidly and thus produces alongwind and crosswind vibrations.

Based on this premise, as it is classical, let us express the wind velocity U of a thunderstorm outflow by the relationship (Fig. 6):

$$U(t) = \overline{U}(t) + U'(t) \tag{9}$$

where $\overline{U}$ is the slowly-varying mean wind velocity extracted here by a running-mean filter with a moving average period $T = 30$ s, whereas U' is the residual turbulent fluctuation expressed as:

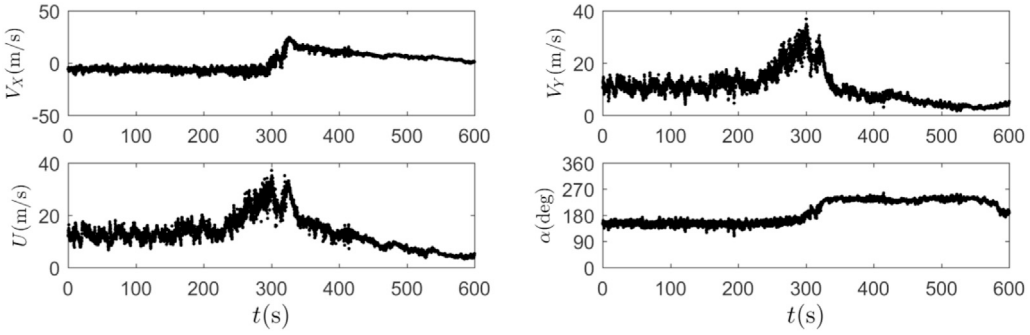

Fig. 7. Application of Eq. (1) to a typical thunderstorm outflow.

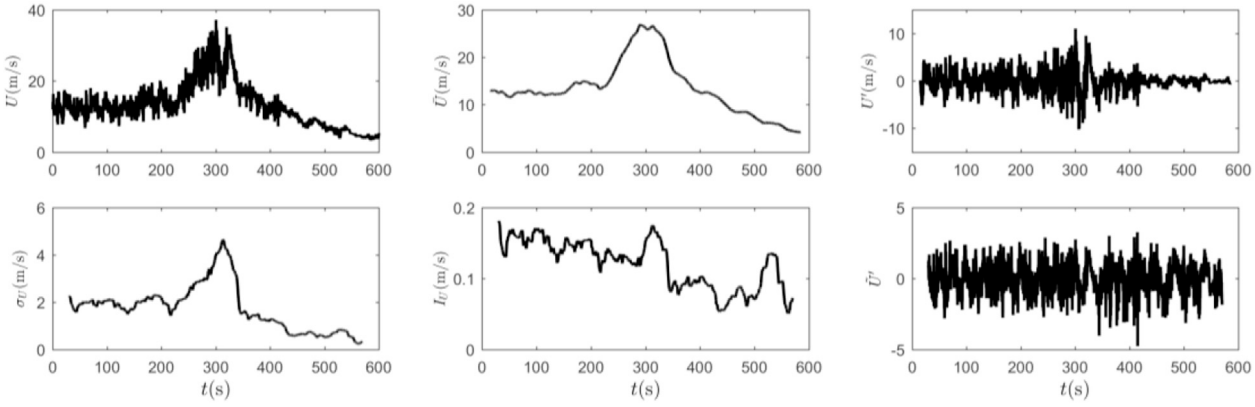

Fig. 8. Application of Eqs. (9) to (12) to a typical thunderstorm outflow.

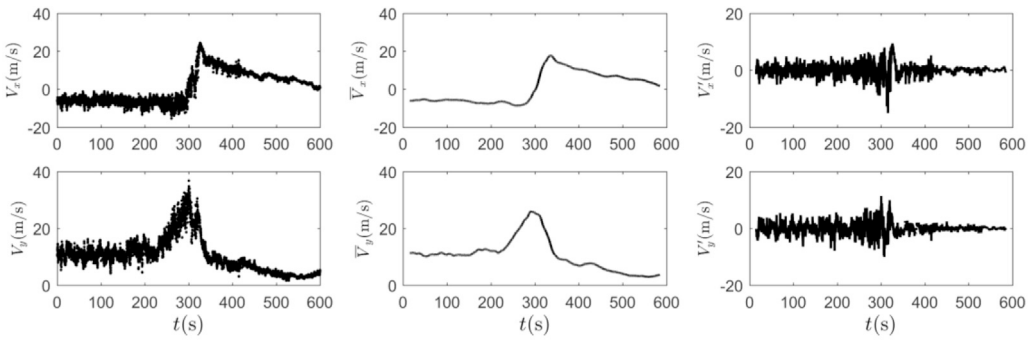

Fig. 9. Application of Eq. (17) to the thunderstorm outflow examined in Section 4.

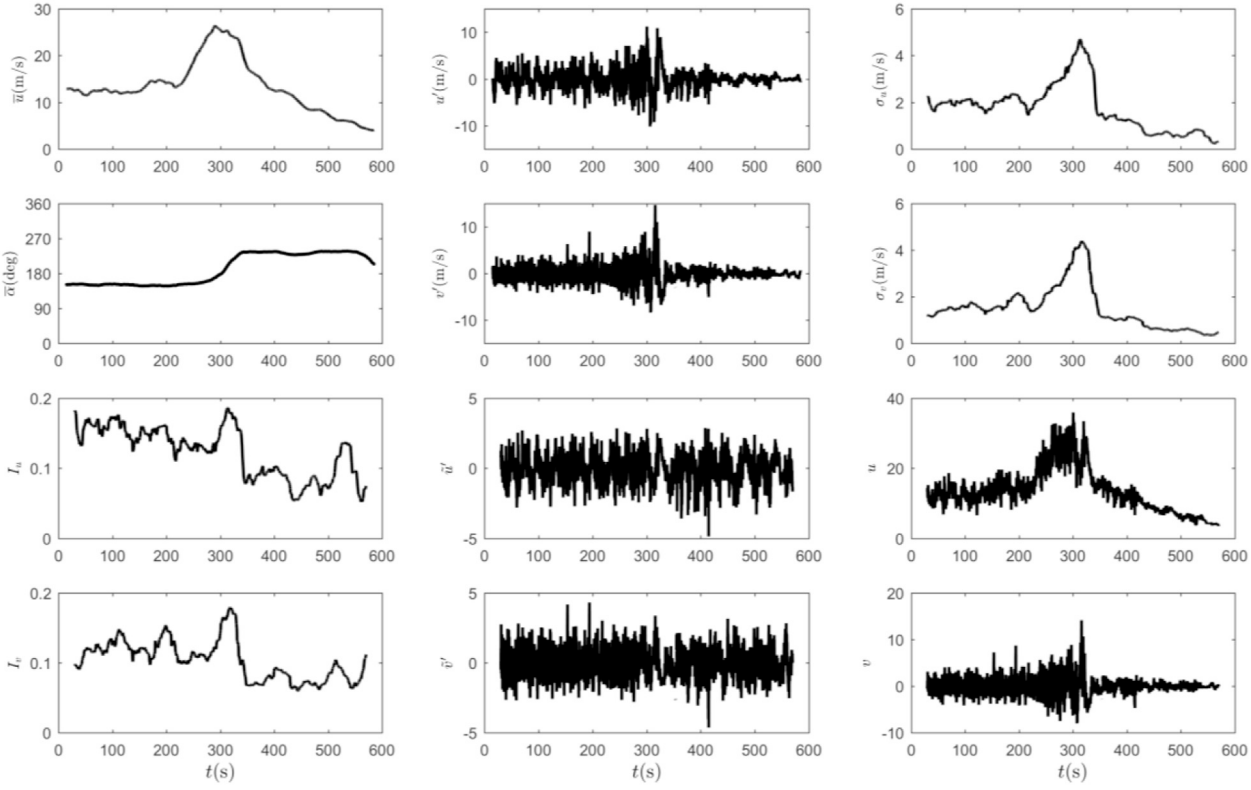

Fig. 10. Application of Eqs. (18)–(22) to the thunderstorm outflow examined in Section4.

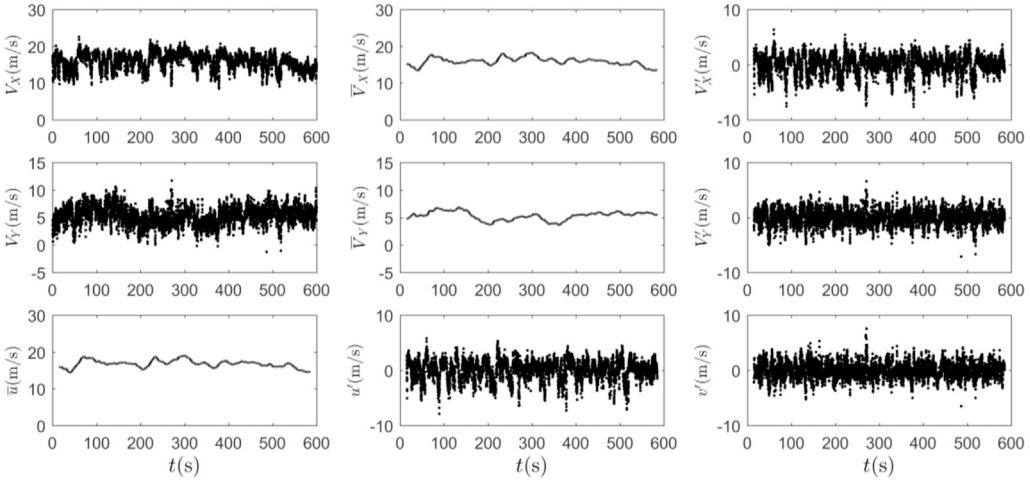

Fig. 11. Application of Eqs. (17)–(22) to the synoptic extra-tropical cyclone examined in Section 3.

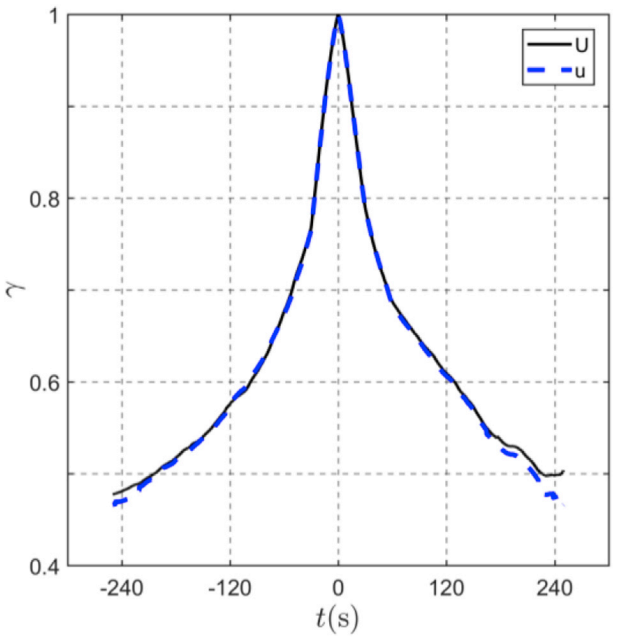

Fig. 12. Ensemble mean value of the normalized slowly-varying mean wind velocity.

$$U^{'}(t) = \sigma_U(t)\tilde{U}^{'}(t) \tag{10}$$

where σ_U is the slowly-varying standard deviation of $U^{'}$, $\tilde{U}^{'}$ is the reduced turbulent fluctuation. This latter quantity is usually modelled as a stationary Gaussian random process with zero mean and unit standard deviation (Chen and Letchford, 2004a; Holmes et al., 2008; Solari et al., 2015a).

Replacing Eq. (10) into Eq. (9), the wind velocity U results:

$$U(t) = \overline{U}(t)\left[1 + I_U(t)\tilde{U}^{'}(t)\right] \tag{11}$$

where:

$$I_U(t) = \sigma_U(t)/\overline{U}(t) \tag{12}$$

is the slowly-varying turbulence intensity.

Let us now express the slowly-varying mean wind velocity and turbulence intensity as:

$$\overline{U}(t) = \overline{U}_{max}\gamma_U(t) \tag{13}$$

$$I_U(t) = \overline{I}_U\mu_U(t) \tag{14}$$

where $\overline{U}_{max}$ is the maximum value of $\overline{U}$ whereas γ_U is a non-dimensional function of t that describes the slow variation of $\overline{U}$, being $\gamma_{U,max} = 1$; $\overline{I}_U$ is the mean value of I_U over ΔT whereas μ_U is a non-dimensional function of t that describes the slow variation of I_U, being $\overline{\mu}_U = 1$.

Replacing Eqs. (13) and (14) into Eq. (11) the wind velocity may be re-written as:

$$U(t) = \overline{U}_{max}\,\gamma_U(t)\left[1 + \overline{I}_U\,\mu_U(t)\tilde{U}^{'}(t)\right] \tag{15}$$

Finally, the gust factor is expressed as:

$$G_U = \widehat{U}/\overline{U}_{max} \tag{16}$$

where $\widehat{U}$ is the peak wind velocity ($\tau = 1$ s).

It is apparent that the above expressions are different from those described in Section 3 not only because they disregard the wind direction. On assuming $T = \Delta T$, namely on identifying the moving average period with the 10-min average period traditionally used for synoptic winds, the model of the thunderstorm outflow depicted above does not provide the classical model of the synoptic wind, where the horizontal turbulent fluctuation is expressed in terms of its longitudinal and lateral components.

Fig. 7 shows the application of Eq. (1) to the wind velocity of a thunderstorm outflow recorded on October 25, 2011 by the anemometer 3 of the Port of La Spezia; the peak wind velocity is $\widehat{U} = 33.98$ m/s. Both the velocity components V_X and V_Y, and thus the velocity U, exhibit typical non-stationary trends characterised by sudden simultaneous ramp-up phases in correspondence of which the wind direction changes of about 90°.

Fig. 8 shows the application of Eqs. (9)–(12) to the same recording. The maximum value of the slowly-varying mean wind velocity is $\overline{U}_{max} = 26.86$ m/s. The slowly-varying turbulence intensity has a mean value $\overline{I}_U = 0.121$; it exhibits a quite unusual decreasing trend. The reduced turbulent fluctuation has nearly zero mean and unit standard deviation; its skewness is $\gamma_U = 0.120$ while its kurtosis is $\kappa_U = 2.895$. As it is classical, the wind direction is no longer considered.

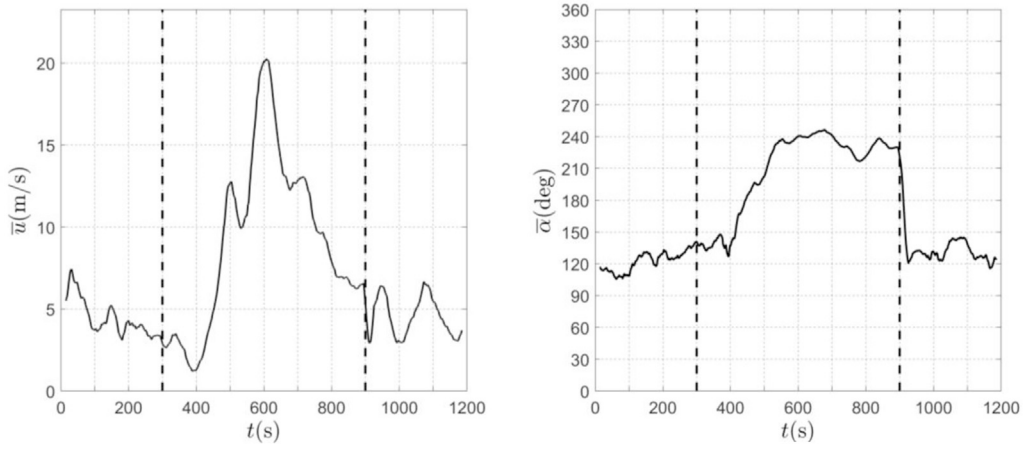

(a) (b)

Fig. 13. 20-min slowly-varying mean wind velocity (a) and direction (b) during a thunderstorm outflow occurred on October 15, 2012 in the Port of La Spezia (the vertical dashed lines include the 10-min period centred around the peak wind velocity).

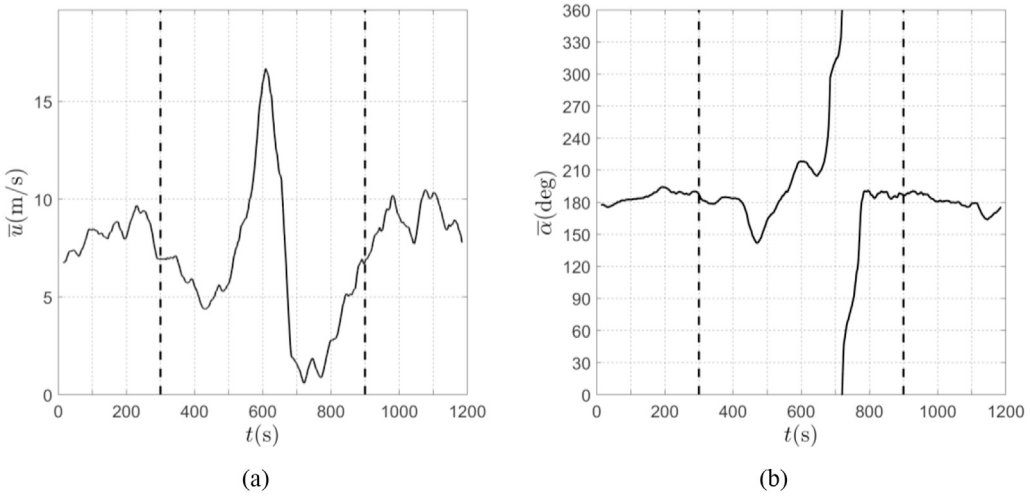

Fig. 14. 20-min slowly-varying mean wind velocity (a) and direction (b) during a thunderstorm outflow occurred on January 18, 2014 in the Port of Livorno (the vertical dashed lines include the 10-min period centred around the peak wind velocity).

Table 2
Number of thunderstorm outflows (%) characterised by given ranges of the maximum shift of the slowly-varying mean wind direction.

Maximum direction shift (deg)	Method 1	Method 2
$\Delta\overline{\alpha} \leq 45$	41 (29%)	92 (65%)
$45 < \Delta\overline{\alpha} \leq 90$	56 (40%)	35 (25%)
$90 < \Delta\overline{\alpha} \leq 180$	30 (21%)	10 (7%)
$\Delta\overline{\alpha} > 180$	14 (10%)	4 (3%)
All	141 (100%)	141 (100%)

5. Novel directional decomposition

In order to overcome the above shortcomings and make the decomposition rule for thunderstorm outflows (Section 4) fully coherent with the one adopted for synoptic phenomena (Section 3), a novel decomposition strategy is herein formulated in which the variation of the wind direction is explicitly taken into account. In this framework, independently of whether the Aeolian phenomenon under examination is a synoptic event or a thunderstorm outflow, the two horizontal components of the wind speed are expressed as (Fig. 4a):

$$\begin{aligned} V_X(t) &= \overline{V}_X(t) + V_X^{'}(t) \\ V_Y(t) &= \overline{V}_Y(t) + V_Y^{'}(t) \end{aligned} \tag{17}$$

where $\overline{V}_X$ and $\overline{V}_Y$ are the slowly-varying mean wind velocity components extracted here by a running-mean filter with a moving average period $T = 30$ s, whereas $V_X^{'}$ and $V_Y^{'}$ are the residual turbulent fluctuations.

It is worth noticing that Eq. (17) identifies with Eq. (2) with the sole difference that the mean wind velocity components depend on time. The same property applies to the following equations in a generalised sense. Adopting this principle Fig. 4 can be retained as the reference scheme also for this section.

Based upon Eq. (17) the slowly-varying mean wind velocity and its slowly varying mean wind direction are given by (Fig. 4a):

$$\begin{aligned} \overline{u}(t) &= \sqrt{\overline{V}_X^2(t) + \overline{V}_Y^2(t)} \\ \overline{\alpha}(t) &= 270 - \mathrm{atan2}\left(\overline{V}_Y(t)/\overline{V}_X(t)\right) \\ \overline{\beta}(t) &= 270 - \overline{\alpha}(t) \end{aligned} \tag{18}$$

where $\overline{\alpha}, \overline{\beta} \in [0 : 360]$. Accordingly, $V_X^{'}$ and $V_Y^{'}$ are projected onto a new Cartesian reference system (x, y), where the x-axis coincides with the direction of $\overline{u} = \overline{u}(t)$ and is rotated $\overline{\beta} = \overline{\beta}(t)$ with respect to the fixed X-axis. Thus (Fig. 4b):

$$\begin{aligned} u^{'}(t) &= V_X^{'}(t)\cos\overline{\beta}(t) + V_Y^{'}(t)\sin\overline{\beta}(t) \\ v^{'}(t) &= -V_X^{'}(t)\sin\overline{\beta}(t) + V_Y^{'}(t)\cos\overline{\beta}(t) \end{aligned} \tag{19}$$

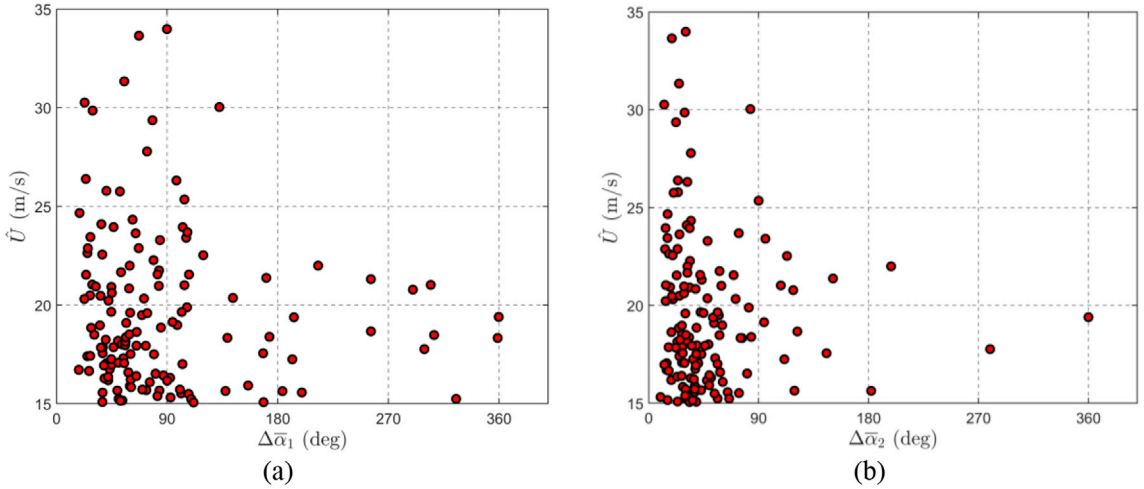

Fig. 15. Peak wind speed $\hat{U}$ as a function of the direction shift: (a) $\Delta\overline{\alpha} = \Delta\overline{\alpha}_1$; (b) $\Delta\overline{\alpha} = \Delta\overline{\alpha}_2$.

Table 3
Ensemble mean value and cov of the turbulence intensity.

Port	Anem. No.	$\bar{I}_U$	cov ($\bar{I}_U$)	$\bar{I}_u$	cov ($\bar{I}_u$)	$\bar{I}_v$	cov ($\bar{I}_v$)
Genoa	1	0.09	0.33	0.09	0.34	0.09	0.32
	2	0.12	0.30	0.13	0.29	0.13	0.27
Livorno	1	0.09	0.26	0.09	0.26	0.09	0.31
	2	0.15	0.15	0.15	0.16	0.14	0.18
	3	0.08	0.22	0.08	0.22	0.08	0.27
	4	0.09	0.27	0.09	0.27	0.08	0.28
	5	0.12	0.28	0.12	0.29	0.12	0.21
Savona	1	0.14	0.19	0.15	0.20	0.13	0.17
	2	0.13	0.00	0.13	0.00	0.12	0.00
	3	0.13	0.41	0.13	0.43	0.14	0.41
	4	0.13	0.22	0.13	0.21	0.13	0.22
	5	0.13	0.40	0.13	0.40	0.13	0.27
La Spezia	2	0.16	0.15	0.17	0.15	0.17	0.18
	3	0.13	0.19	0.13	0.20	0.12	0.20
All ports		0.12	0.32	0.12	0.33	0.11	0.34

where u' and v' are the longitudinal and lateral turbulent fluctuations. Eq. (19) can also be re-written as:

$$\begin{aligned} u'(t) &= \sigma_u(t)\tilde{u}'(t) \\ v'(t) &= \sigma_v(t)\tilde{v}'(t) \end{aligned} \tag{20}$$

where σ_u and σ_v are the slowly varying standard deviations of u' and v', $\tilde{u}'$ and $\tilde{v}'$ are the reduced longitudinal and lateral turbulent components. The prosecution of this paper proves that these latter quantities can be modelled as un-correlated stationary Gaussian random processes with zero mean and unit standard deviation.

Thanks to Eqs. (18)–(20) the longitudinal and lateral components of the wind velocity can be expressed as:

$$\begin{aligned} u(t) &= \bar{u}(t) + u'(t) = \bar{u}(t)\left[1 + I_u(t)\tilde{u}'(t)\right] \\ v(t) &= v'(t) = \bar{u}(t)I_v(t)\tilde{v}'(t) \end{aligned} \tag{21}$$

where I_u and I_v are the slowly-varying longitudinal and lateral turbulence intensities:

$$\begin{aligned} I_u(t) &= \sigma_u(t)/\bar{u}(t) \\ I_v(t) &= \sigma_v(t)/\bar{u}(t) \end{aligned} \tag{22}$$

Eqs. (17)–(22) represent a full generalization of Eqs. (2)–(7) with the key remark that the mean quantities, the standards deviations and the turbulence intensities are now slowly-varying function of time as well as the direction of the mean wind speed. It follows that the longitudinal and lateral turbulence components of the wind velocity are aligned with a couple axes (x, y) whose direction is a slowly-varying function of time.

Likewise Eqs. (13) and (14), the slowly-varying mean wind speed and the slowly-varying turbulence intensities can be expressed as:

$$\bar{u}(t) = \bar{u}_{max}\gamma_u(t) \tag{23}$$

$$\begin{aligned} I_u(t) &= \bar{I}_u\mu_u(t) \\ I_v(t) &= \bar{I}_v\mu_v(t) \end{aligned} \tag{24}$$

where $\bar{u}_{max}$ is the maximum value of $\bar{u}$ whereas γ_u is a non-dimensional function of t that describes the slow variation of $\bar{u}$, being $\gamma_{u,max} = 1$; $\bar{I}_u$ and $\bar{I}_v$ are the mean values of I_u and I_v in ΔT, whereas μ_u and μ_v are non-dimensional functions of t that describe the slow variation of I_u and I_v, being $\bar{\mu}_u = \bar{\mu}_v = 1$.

In a similar way to Eq. (15), replacing Eqs. (23) and (24) into Eq. (21) the longitudinal and lateral components of the wind velocity may be re-written as:

$$\begin{aligned} u(t) &= \bar{u}(t)\left[1 + I_u(t)\tilde{u}'(t)\right] = \bar{u}_{max}\gamma_u(t)\left[1 + \bar{I}_u\mu_u(t)\tilde{u}'(t)\right] \\ v(t) &= \bar{u}(t)I_v(t)\tilde{v}'(t) = \bar{u}_{max}\gamma_u(t)\bar{I}_v\mu_v(t)\tilde{v}'(t) \end{aligned} \tag{25}$$

Finally, the gust factor is expressed by the relationship:

$$G_u = \hat{u}/\bar{u}_{max} \tag{26}$$

where $\hat{u}$ is the peak longitudinal velocity ($\tau = 1$ s).

It is worth noting that, on assuming $T = \Delta T$, namely identifying the moving average period with the 10-min average period, this model provides the classical model for synoptic wind speeds as a particular case. In this case, $\bar{u}$, σ_u, σ_v, I_u and I_v are constant quantities whereas $\bar{u}_{max} = \bar{u}$, $\gamma = \mu_u = \mu_v = 1$.

Fig. 9 shows the application of Eq. (17) to the wind velocity of the thunderstorm outflow already analysed in Section 4. Similarly, Fig. 10 shows the application of Eqs. (18)–(22). The maximum value of the slowly-varying mean wind velocity is $\bar{u}_{max} = 26.39$ m/s; it is slightly different from the value $\bar{U}_{max} = 26.86$ m/s provided by the classical approach. The mean values of the longitudinal and lateral turbulence intensities are $\bar{I}_u = 0.123$ and $\bar{I}_v = 0.104$, respectively; their ratio, $\bar{I}_v/\bar{I}_u = 0.85$, is greater than the reference value $I_v/I_u = 0.75$ commonly adopted for synoptic winds. The reduced longitudinal and lateral turbulence components have both nearly zero mean and unit standard deviation; their skewness values are $\gamma_u = -0.129$ and $\gamma_v = 0.129$ while the kurtosis values are $\kappa_u = 2.924$ and $\kappa_v = 2.996$; the cross-correlation coefficient is $\rho_{uv} = -0.152$.

Fig. 11 shows the application of Eqs. (17)–(22) to the wind velocity of

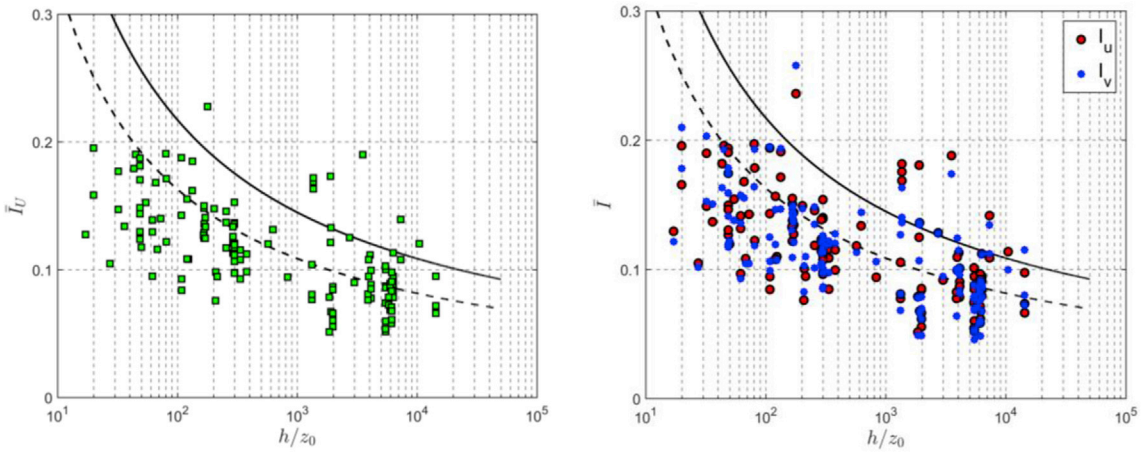

Fig. 16. Mean value of the turbulence intensity as a function of h/z_0: (a) $\bar{I}_U$; (b) $\bar{I}_u$ and $\bar{I}_v$.

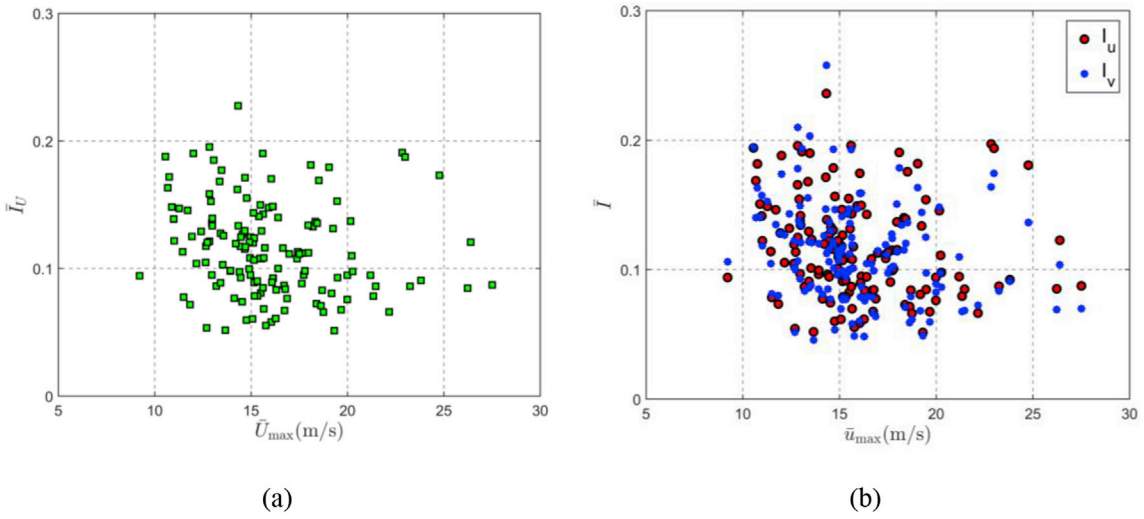

Fig. 17. Mean value of the turbulence intensity as a function of the maximum mean wind velocity: (a) $\bar{I}_U$; (b) $\bar{I}_u$ and $\bar{I}_v$.

the synoptic extra-tropical cyclone already analysed in Section 3. In this case, the slowly varying mean wind velocity is characterised by a low-frequency harmonic content (slowly-varying long waves), previously embedded in the classical residual turbulent fluctuations, while the new residual turbulent fluctuations exhibit only a dominant high-frequency harmonic content (rapidly-varying short oscillations). The maximum value of the slowly-varying mean wind velocity is $\overline{u}_{max} = 16.80$ m/s; as expected, it is slightly greater than the constant value $\overline{u} = 16.71$ m/s, since it takes into account the slowly-varying long waves previously embedded in the turbulent fluctuations. The mean values of the longitudinal and lateral turbulence intensities are $\bar{I}_u = 0.10$ and $\bar{I}_v = 0.08$, respectively; their ratio, $\bar{I}_v/\bar{I}_u = 0.82$, is greater than the previous value $I_v/I_u = 0.76$ since excluding the slowly-varying long waves from the turbulent fluctuations they tend to the isotropic condition typical of the inertial sub-range. The reduced longitudinal and lateral turbulence components have nearly zero mean and unit standard deviation; their skewness and kurtosis values are $\gamma_u = -0.61$, $\gamma_v = 0.13$, $\kappa_u = 3.45$, $\kappa_v = 3.58$; the cross-correlation coefficient is $\rho_{uv} = -0.03$.

6. Statistical properties of the thunderstorm outflows

Having available 141 thunderstorm outflow recordings involving rapid variations in speed and often in direction, each of them has been first decomposed into component signals whose properties have been examined; this operation has been carried out by means of the classical (Section 4) and novel (Section 5) rule. Subsequently, these properties have been analysed as a whole in statistical form. Finally, the results are compared and discussed. In this framework, the prosecution of this section deals with the slowly-varying mean wind speed (Section 6.1) and direction (6.2), the turbulence intensity (Section 6.3), the reduced turbulent fluctuations (Section 6.4), their integral length scales (Section 6.5) and power spectral densities (Section 6.6), the turbulence intensity modulation (Section 6.7) and the gust factor (Section 6.8). It is worth noticing that the application of the classical method may involve some slight differences respect to the results obtained by Zhang et al. (2018a) and even more by Solari et al. (2015a); this happens because, on passing the time, the data and dataset have been progressively improved.

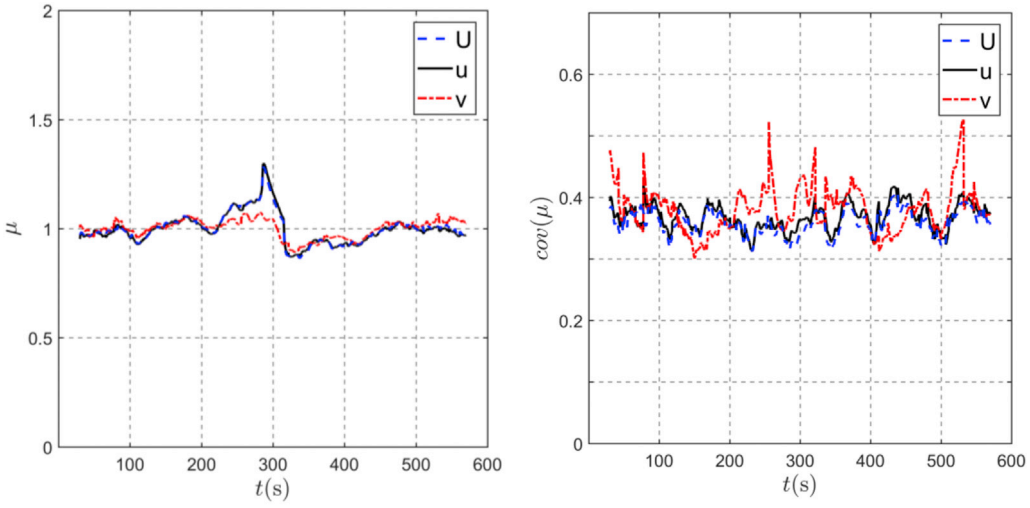

Fig. 18. Ensemble mean (a) and cov (b) values of μ.

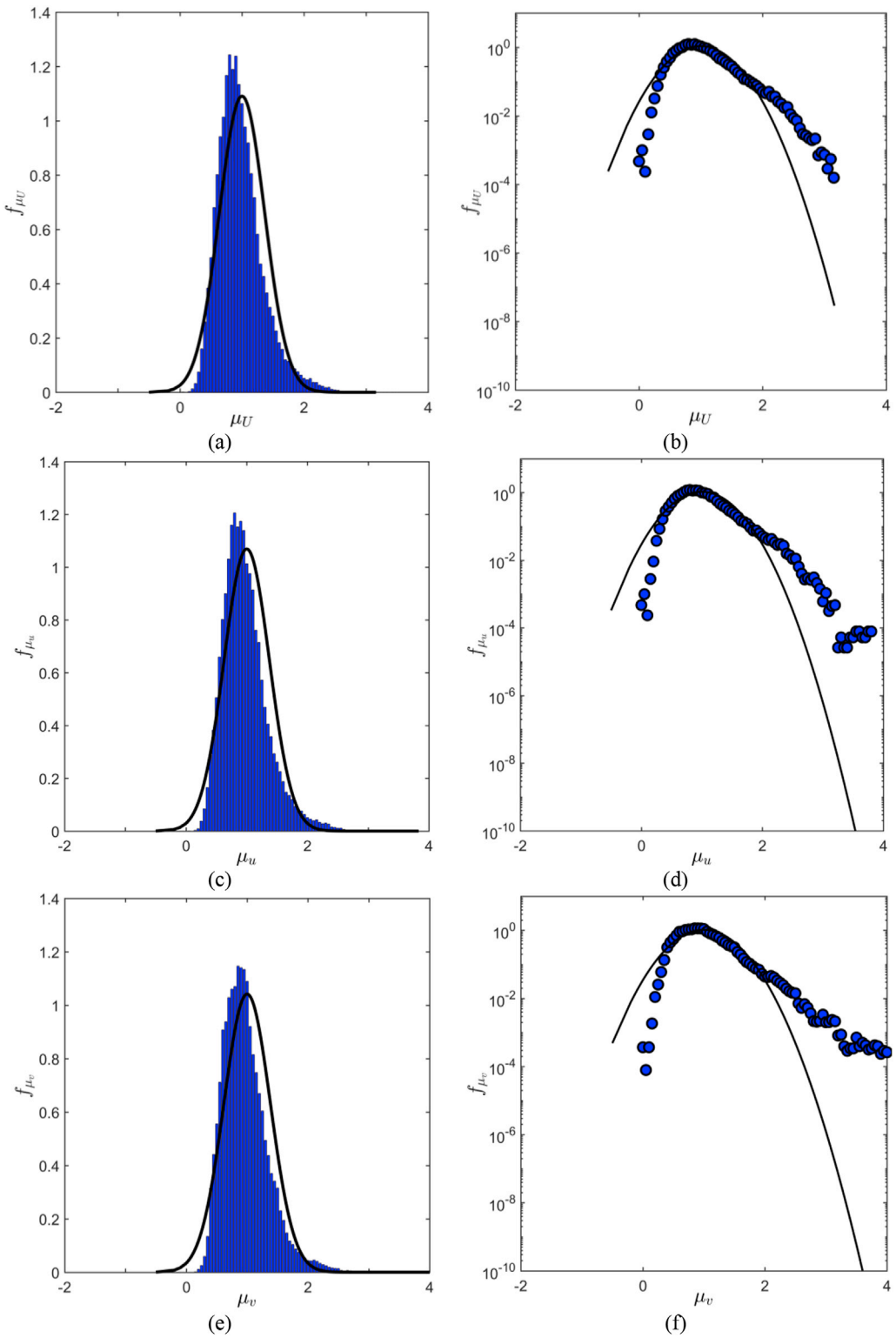

Fig. 19. PDF of μ_U, μ_u and μ_v: decimal (a) (c) (e) and logarithmic (b) (d) (f) ordinate.

6.1. Slowly-varying mean wind velocity

The comparison between the slowly-varying mean wind velocity evaluated by means of the classical, $\overline{U}_{max}$, and directional, $\overline{u}_{max}$, decomposition rules proves that they are, on average, very close to each other: the average value of their ratios over the ensemble of the analysed records is $< \overline{u}_{max}/\overline{U}_{max} > = 0.99$. Fig. 12 shows the average value of the non-dimensional functions $\gamma_U(t)$ (Eq. (13), black solid line) and $\gamma_u(t)$ (Eq. (23), blue dashed line) over all the thunderstorm outflow records investigated; they are characterised by a prominent peak that sums up the essential features of the sudden ramp-up and slow-down of the wind speed corresponding to the passage of a gust front. It is apparent that the classical decomposition rule and the new directional one provide almost overlapped results in proximity of the peak whereas small differences occur on the tails.

6.2. Slowly-varying mean wind direction

According to the classical decomposition rule, the wind direction of the thunderstorm outflows is usually examined qualitatively, but later disregarded quantitatively. This unavoidably leads to consider the wind direction, more or less implicitly, as invariant with time. The dominant property of the new decomposition strategy is its ability to extract and embed the slowly-varying mean wind direction $\overline{\alpha}$ or $\overline{\beta}$ (Eq. (18)) within the wind velocity model.

This fact is relevant because, when a thunderstorm outflow occurs, the slowly-varying mean wind direction often changes suddenly, and the rate of this change depends on the translation of the thunderstorm cell with respect to the anemometer that registers the record as well as on the background wind speed – namely the wind speed associated with the synoptic weather condition in which the thunderstorm takes place - before and after the downburst, which in principle could be different from each other. This situation may make difficult to distinguish between the rate of change due to the thunderstorm outflow alone and the rate of change that occurs due to the evolution of the weather conditions.

The examination of the slowly-varying mean wind direction of the thunderstorm outflow records considered here depicts complex and varied trends that make anything but simple to classify these phenomena according to their shift in wind direction.

Figs. 13 and 14 show two examples of thunderstorm outflows during which the background wind velocity is almost unchanged before and after the gust front passage; this can happen, as an instance, during fair weather conditions, when some forcing mechanism triggers the formation of a deep convective cell. In both cases the sudden jump of the slowly-varying mean wind velocity is accompanied by a relevant change of the slowly-varying mean wind direction. During the event depicted in Fig. 13 the slowly-varying mean wind direction exhibits a rotation around 120°, which mainly occurs before the peak wind speed. Conversely, the event depicted in Fig. 14 gives rise to a wind rotation around 60° before the peak wind speed; after such peak, the wind rotation continues clockwise to complete a full angle.

Table 2 implements a pair of conventional attempts to quantify the rate of change of the slowly-varying mean wind direction, $\Delta\overline{\alpha}$, by providing the number of events characterised by different ranges of this quantity. In the column referred to as Method 1, $\Delta\overline{\alpha} = \Delta\overline{\alpha}_1$ corresponds to the maximum shift of the wind direction in the 10-min period centred around the peak wind speed. In the column referred to as Method 2, $\Delta\overline{\alpha} = \Delta\overline{\alpha}_2$ corresponds to the maximum shift of the wind direction in the 5-min period preceding the peak wind speed. According to Method 1, most of the examined events (90%) has a rate of change $\Delta\overline{\alpha}_1$ in the range from 0 to 180 deg. According to Method 2, most of the examined events (90%) has a rate of change $\Delta\overline{\alpha}_2$ in the range from 0 to 90 deg. Moreover, it has been verified that most of the shift of the slowly-varying mean wind direction occurs during the ramp-up phase of the wind speed that characterises the passage of the gust front.

Fig. 15a shows the peak wind speed $\widehat{U}$ as a function of the direction shift $\Delta\overline{\alpha}_1$. Three remarks stand out: 1) none of the examined events is characterised by $\Delta\overline{\alpha}_1 < 15°$, which corresponds to nearly straight winds; 2) a limited amount of events, 15%, involves $\Delta\overline{\alpha}_1 > 135°$; none of them exceeds the peak wind speed $\widehat{U} = 25$ m/s; thus, they correspond to rather weak winds; 3) the largest amount of events, 85%, falls in the range $\Delta\overline{\alpha}_1$ between 15 and 135°; here, no apparent correlation exists between $\widehat{U}$ and $\Delta\overline{\alpha}_1$; despite this remark, the three most intense events, those exceeding $\widehat{U} = 30$ m/s, fall in the range $\Delta\overline{\alpha}_1$ between 50 and 90°.

Fig. 15b shows the peak wind speed $\widehat{U}$ as a function of the direction shift $\Delta\overline{\alpha}_2$. The comparison with Fig. 15a shows an apparent compaction of the data towards the smaller values of the direction shift. Also in this case, no apparent correlation exists between $\widehat{U}$ and $\Delta\overline{\alpha}_2$; despite this remark, the three most intense events, those exceeding $\widehat{U} = 30$ m/s, fall in the range $\Delta\overline{\alpha}_2$ between 20 and 30°.

This matter deserves further studies with a prominent focus on separating the wind speed components related to the downdraft, to the background flow into which it is embedded and to the translational speed of the thunderstorm cell (Asano et al., 2019; Romanic et al., 2019), recognizing the interactions between the different components of the wind speed.

6.3. Turbulence intensity

As described in Sections 4 and 5, the longitudinal and lateral slowly-varying turbulence intensities, I_u and I_v, can be extracted by means of the directional decomposition rule through Eq. (22) whereas the turbulent intensity based on the classical method, I_U, can be evaluated by Eq. (12). It is worth noting that in some cases the turbulent intensity time-histories exhibit abnormal large values and even sharp peaks in correspondence of very small values of the slowly-varying mean wind velocity, sometimes tending to zero. In this study, differently from the previous ones (Solari et al., 2015a; Zhang et al., 2018a), large turbulence intensities (greater than 0.2) related to small slowly-varying mean wind velocities (less than 5 m/s) have been disregarded.

Table 3 shows the average values and the coefficients of variation (cov) of $\bar{I}_U$, $\bar{I}_u$ and $\bar{I}_v$ corresponding to the thunderstorm outflows investigated. The ensemble values, shown in the last row, exhibit some relevant properties. First, the $\bar{I}_U$ and $\bar{I}_u$ values are very similar; thus the turbulence intensity evaluated by the classical decomposition rule closely approximates the longitudinal turbulence intensity extracted through the new rule. Second, differently from classical analyses carried out for synoptic winds, the $\bar{I}_u$ and $\bar{I}_v$ values related to thunderstorm outflows are almost equal: .. is slightly greater than $\bar{I}_v$ whereas cov ($\bar{I}_u$) and cov ($\bar{I}_v$)are nearly the same.

This latter circumstance may be interpreted based on the remark that in the case of synoptic winds the residual turbulence derives from averaging the wind speed over a 10-min period, so it contains a relevant amount of low frequency harmonic content (Section 3). In the case of thunderstorm outflows (Sections 4 and 5) the use of a mobile mean wind speed with an averaging period $T = 30$ s elides the low frequency harmonic content and limits it, indicatively, to the inertial sub-range, where turbulence is locally isotropic.

In order to investigate the dependence of the mean value of the turbulence intensity of thunderstorm outflows on the height h AGL and on the roughness length z_0, (Xu and Hangan, 2008; Lombardo et al., 2014), Fig. 16 shows $\bar{I}_U$, $\bar{I}_u$ and $\bar{I}_v$ as a function of h/z_0. Here, the z_0 values have been evaluated as described by Solari et al. (2015a), referring to neutral synoptic wind velocity profiles in equilibrium with the local topography and the upwind roughness features (Engineering Sciences Data Unit, 1993; Castino et al., 2003; Burlando et al., 2013). The solid and dashed lines correspond, respectively, to the expressions $\bar{I}_u = 1/\ln(h/z_0)$ and $\bar{I}_v = 0.75\bar{I}_u$ commonly used for synoptic events and neutral conditions (Solari and Piccardo, 2001). It is worth noting, however, that these expressions are calibrated to fluctuations related to 10-min mean wind velocities whereas in Fig. 16 the fluctuations correspond to a mean wind velocity extracted through a moving average period $T = 30$ s. This is the main reason why turbulence intensity values related to thunderstorms are generally lower than these reference curves. It is also worth noting

Table 4
Ensemble Mean and Std of the mean, standard deviation, skewness and kurtosis (m, σ, γ κ) of μ_U, μ_u and μ_v.

	Parameter	m	σ	γ	κ
μ_U	Mean	1.000	0.353	0.744	3.431
	Std	0.000	0.099	0.537	1.275
μ_u	Mean	1.000	0.360	0.780	3.560
	Std	0.000	0.102	0.564	1.523
μ_v	Mean	1.000	0.368	0.752	3.520
	Std	0.000	0.111	0.595	1.873

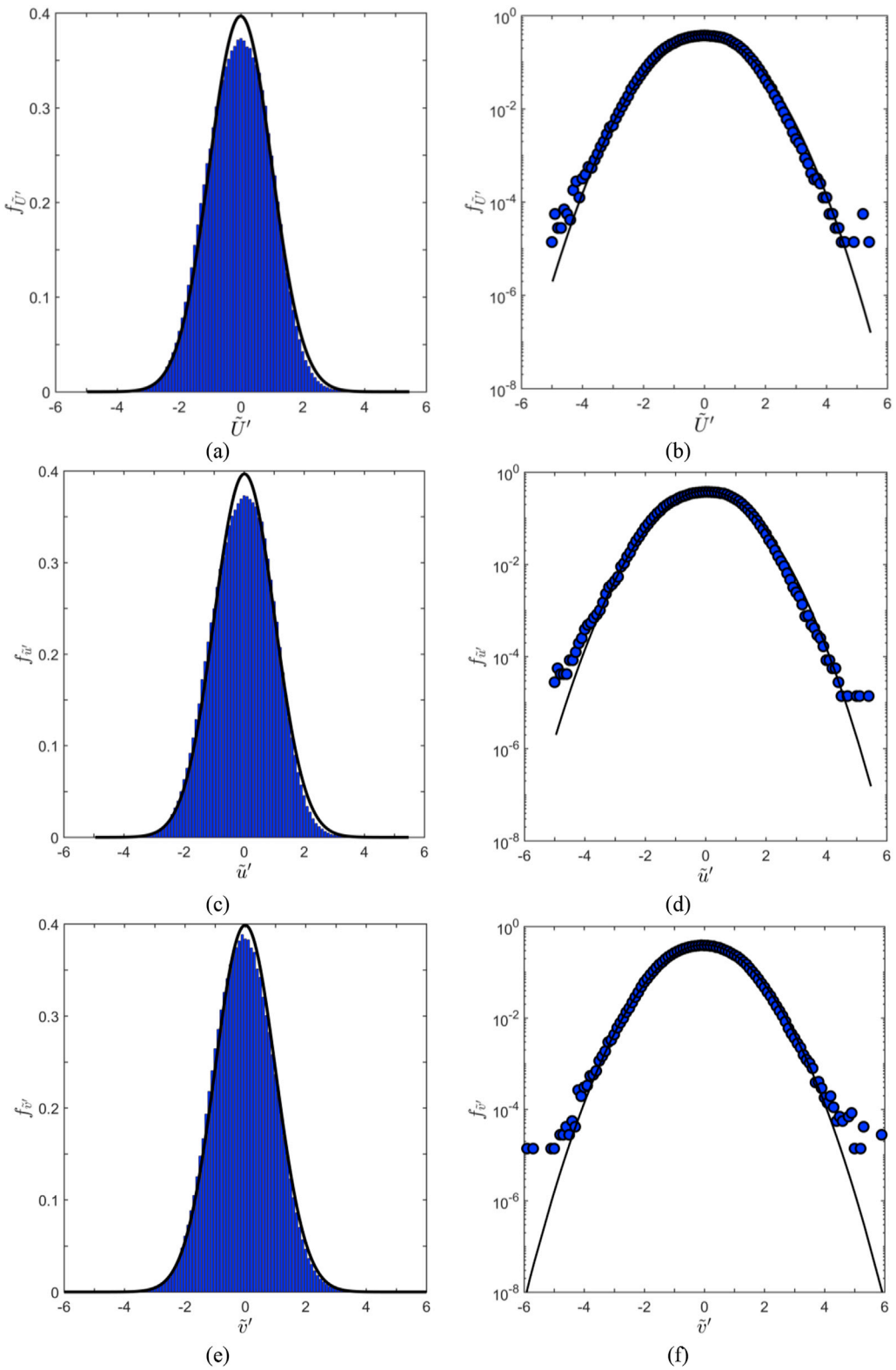

Fig. 20. PDF of $\tilde{U}'$, $\tilde{u}'$ and $\tilde{v}'$: decimal (a) (c) (e) and logarithmic (b) (d) (f) ordinate.

that $\bar{I}_U$, $\bar{I}_u$ and $\bar{I}_v$ exhibit similar values (Table 3) and trends characterised by a moderate decrease on increasing h/z_0; this trend was not present in Solari et al. (2015a) and only slightly evident in Zhang et al. (2018a); it is possible that the improved quality of the dataset and the removal of abnormally large values of the turbulence intensity reveal now a property that was, initially, not or slightly appreciable.

Fig. 17 shows that $\bar{I}_U$, $\bar{I}_u$ and $\bar{I}_v$ don't exhibit any relevant dependence on the maximum value of the slowly-varying mean wind velocity.

Fig. 18 shows the ensemble average (a) and the cov (b) values of $\mu_U(t)$, $\mu_u(t)$ and $\mu_v(t)$. The diagrams related to $\mu_U(t)$ and $\mu_u(t)$ are almost perfectly overlapped; those corresponding to $\mu_v(t)$ shows limited detachments from the previous ones; all in all they are weakly dependent on

Table 5
Ensemble Mean and Std of the mean, standard deviation, skewness and kurtosis (m, σ, γ κ) of $\tilde{U}'$, $\tilde{u}'$ and $\tilde{v}'$.

	Parameter	m	σ	γ	κ
$\tilde{U}'$	Mean	−0.010	1.005	−0.068	2.835
	Std	0.020	0.012	0.153	0.255
$\tilde{u}'$	Mean	0.011	1.005	−0.089	2.843
	Std	0.023	0.011	0.153	0.263
$\tilde{v}'$	Mean	−0.001	1.001	0.018	3.000
	Std	0.018	0.010	0.123	0.504

Table 6
Ensemble coefficient of correlation of $\tilde{u}'$ and $\tilde{v}'$.

Port	Anem. No.	ρ_{uv}
Genoa	1	−0.14
	2	−0.03
Livorno	1	0.01
	2	0.01
	3	−0.01
	4	0.00
	5	−0.01
La Spezia	2	0.02
	3	−0.05
Savona	1	0.00
	2	−0.01
	3	0.00
	4	0.03
	5	0.04
	2	0.02
All ports		−0.01

time, with the exception of a small around of $t = 300$ s where $\mu_U(t)$ and $\mu_u(t)$are significantly greater than 1. Thus, they may be reasonably regarded as sample functions of a stationary process.

As already noted by Zhang et al. (2018a) for the classical decomposition rule, also for the new directional one the probability density function (PDF) f of $\mu_U(t), \mu_u(t)$and $\mu_v(t)$ are non-Gaussian. Fig. 19 elucidates this property by comparing the PDF of these quantities with reference Gaussian PDFs with the same mean and cov values. Table 4 strengthens this remark by showing the mean value (Mean) and the standard deviation (Std) of the mean (m), standard deviation (σ), skewness (γ) and kurtosis (κ) of μ_U, μ_u and μ_v: the detachment of the skewness and kurtosis values from 0 to 3, respectively, is apparent.

6.4. Reduced turbulent fluctuations

Solari et al. (2015a) proved a result widely shared in literature: the reduced turbulent fluctuation $\tilde{U}'(t)$ can be reasonably modelled as a stationary Gaussian random process with zero mean and unit standard deviation. The analysis of an enlarged dataset of thunderstorm outflows (Zhang et al., 2018a) confirmed this remark. The application of the novel directional decomposition rule to a refined dataset of events shows that the above property can be extended to the longitudinal and lateral reduced turbulence components $\tilde{u}'$ and $\tilde{v}'$ (Fig. 20 and Table 5). In addition, likewise for synoptic winds, Table 6 shows that the longitudinal and lateral reduced turbulence components are, to a very good extent, un-correlated.

6.5. Integral length scale

The integral length scale and the power spectral density (PSD) of the longitudinal and lateral reduced turbulence components, $\tilde{u}'$ and $\tilde{v}'$, are determined here for a highly controlled sub-set of 74 thunderstorm outflow records including an extremely low number of missing values; in the few points in which the time-histories are interrupted, their continuity is recovered through linear interpolation.

Table 7 shows the mean value and the cov of the integral length scales L_U, L_u and L_v of $\tilde{U}'$, $\tilde{u}'$ and $\tilde{v}'$ as detected by each anemometer and the whole network. Their time scales T_U, T_u and T_v have been first estimated by integrating the normalized auto-correlation functions from 0 until the time lag for which their values drop to 0.05 (Flay and Stevenson, 1988); the integral length scales are then determined by means of the Taylor's hypothesis: $L_U = \overline{U}_{max} T_U$, $L_u = \overline{u}_{max} T_u$ and $L_v = \overline{u}_{max} T_v$.

In terms of ensemble mean values, $\langle L_U \rangle = 26.78$ m is similar to $\langle L_u \rangle = 25.66$ m, which is slightly greater than $\langle L_v \rangle = 20.83$ m. In terms of spread, $\mathrm{cov}(L_U) = 0.23$ is similar to $\mathrm{cov}(L_u) = 0.24$, which is slightly smaller than $\mathrm{cov}(L_v) = 0.29$.

Fig. 21 shows that L_U, L_u and L_v do not exhibit any significant dependence on h/z_0. Fig. 22 shows that L_U, L_u and L_v increase on increasing the maximum value of the slowly-varying mean wind velocity. This result matches with the one provided by Engineering Sciences Data Unit (1993) for synoptic winds and neutral atmospheric conditions.

6.6. Power spectral density

Approaching the thunderstorm outflow decomposition by means of the classical rule, Zhang et al. (2018a) demonstrated that expressing the PSD of $\tilde{U}'$ as a function of the reduced frequency $f_U = nz/\overline{U}_{max}$, being z the height of the anemometer, is not appropriate. Better results may be obtained by expressing such PSD as a function of the reduced frequency $f_U = nL_U/\overline{U}_{max}$, being L_U the integral length scale of $\tilde{U}'$ obtained through its auto-correlation function. The application of the novel directional decomposition rule shows that the same property is valid also for $\tilde{u}'$ and $\tilde{v}'$.

Fig. 23a,b,c show the PSD of $\tilde{U}'$, $\tilde{u}'$ and $\tilde{v}'$ as a function of $f_U =$

Table 7
Ensemble mean value and cov of the integral length scale of the reduced turbulent fluctuation.

Port	Anem.No.	$\langle L_U \rangle$(m)	cov(L_U)	$\langle L_u \rangle$(m)	cov(L_u)	$\langle L_v \rangle$(m)	cov(L_v)
Genoa	1	33.13	0.20	32.35	0.21	25.98	0.23
	2	23.47	0.35	22.73	0.33	18.65	0.46
Livorno	1	27.54	0.14	25.37	0.09	19.51	0.04
	2	24.33	0.24	22.96	0.23	17.34	0.17
	3	28.28	0.22	27.18	0.24	21.71	0.32
	4	29.94	0.13	29.27	0.13	23.56	0.27
	5	31.18	0.26	31.09	0.26	27.53	0.20
Savona	1	27.11	0.31	26.59	0.32	17.48	0.31
	2	–	–	–	–	–	–
	3	25.48	0.21	25.47	0.22	20.40	0.12
	4	25.23	0.07	24.86	0.07	20.57	0.07
	5	24.77	0.00	24.33	0.00	22.10	0.00
La Spezia	2	25.29	0.30	24.04	0.30	22.68	0.33
	3	25.66	0.23	23.81	0.23	18.41	0.28
All ports		26.78	0.23	25.66	0.24	20.83	0.29

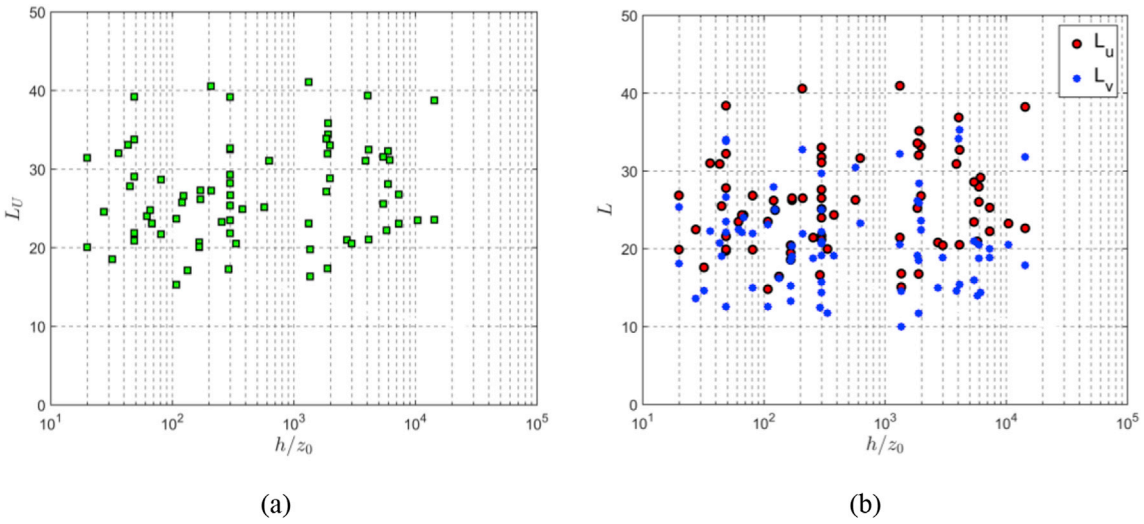

Fig. 21. Integral length scale as a function of h/z_0: (a) L_U; (b) L_u and L_v.

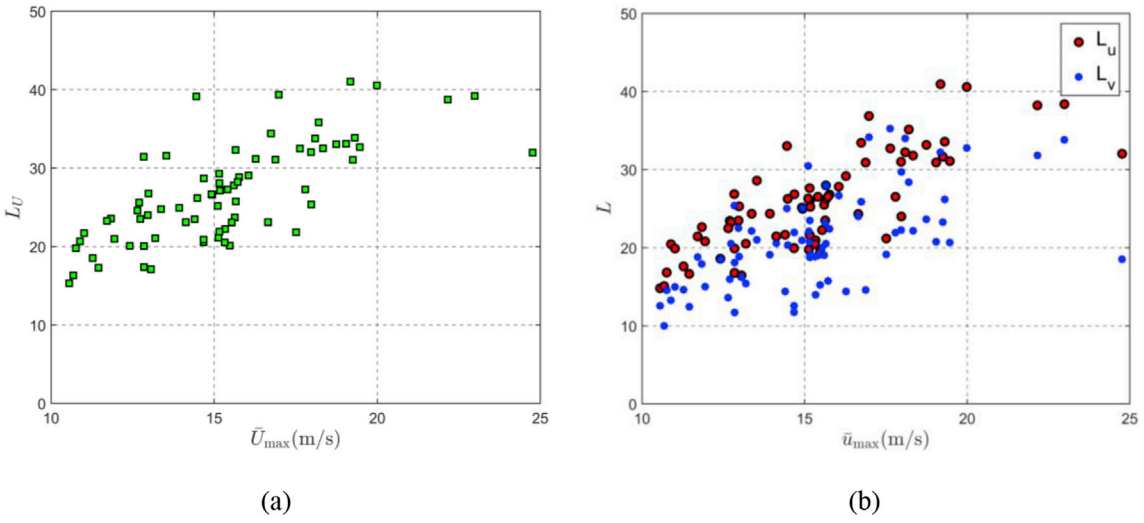

Fig. 22. Integral length scale as a function of the maximum value of the slowly-varying mean wind velocity: (a) L_U; (b) L_u and L_v.

$nL_U/\overline{U}_{max}$, $f_u = nL_u/\overline{u}_{max}$ and $f_v = nL_v/\overline{u}_{max}$, respectively; each scheme provides the mean PSD for every anemometer. Fig. 23d compares the PSD of $\tilde{U}'$, $\tilde{u}'$ and $\tilde{v}'$ averaged over the ensemble of all the anemometers. On the one hand they confirm the reliability of the parameterization adopted here and by Zhang et al. (2018a). On the other hand they show that the PSD of $\tilde{U}'$ is almost perfectly overlapped with the PSD of $\tilde{u}'$; the PSD of $\tilde{v}'$ exhibits some limited detachments from the previous ones.

6.7. Turbulence intensity modulation

Though $\tilde{U}'(t)$, $\tilde{u}'(t)$ and $\tilde{v}'(t)$ are well represented by Gaussian (rapidly-varying) random processes, according to Eqs. (15) and (25) they are modulated by the non-Gaussian (slowly-varying) random processes $\mu_U(t)$, $\mu_u(t)$ and $\mu_v(t)$. Therefore, $\mu_U(t)\tilde{U}'(t)$, $\mu_u(t)\tilde{u}'(t)$ and $\mu_v(t)\tilde{v}'(t)$ are non-Gaussian random processes. Table 8 shows the mean value and the std of the mean, standard deviation, skewness and kurtosis of $\mu_U(t)\tilde{U}'(t)$, $\mu_u(t)\tilde{u}'(t)$ and $\mu_v(t)\tilde{v}'(t)$, exhibiting a relevant agreement between the statistical moments of $\mu_U(t)\tilde{U}'(t)$ and $\mu_u(t)\tilde{u}'(t)$; the statistical moments of $\mu_v(t)\tilde{v}'(t)$ show some differences. Fig. 24 points out the detachment between the PDF of $\mu_U(t)\tilde{U}'(t)$, $\mu_u(t)\tilde{u}'(t)$ and $\mu_v(t)\tilde{v}'(t)$ and the reference Gaussian models. Fig. 25 proves that the PSDs of $\mu_U(t)\tilde{U}'(t)$ and $\mu_u(t)\tilde{u}'(t)$ are almost exactly overlapped whereas the PSD of $\mu_v(t)\tilde{v}'(t)$ exhibits some slight detachment from the previous ones. The PSDs of $\tilde{U}'(t)$, $\tilde{u}'(t)$ and $\tilde{v}'(t)$ are very close to the PSDs of their modulations.

6.8. Gust factor

Table 9 summarizes the mean value and the cov of the gust factors G_U (Eq. (16)) and G_u (Eq. (26)), showing an almost perfect matching. Coherently with the results obtained by Zhang et al. (2018a), Fig. 26 shows that both gust factors do not exhibit any clear correlation with h/z_0. Fig. 27 shows that the same quantities slightly decrease on increasing the maximum value of the slowly-varying mean wind velocity.

7. Conclusions and prospects

This paper proposes a novel decomposition rule of the horizontal component of the wind speed that can be used to analyse measured records and to develop analytical models. Likewise for synoptic winds, but diversely from the tradition in thunderstorm outflows, this rule takes

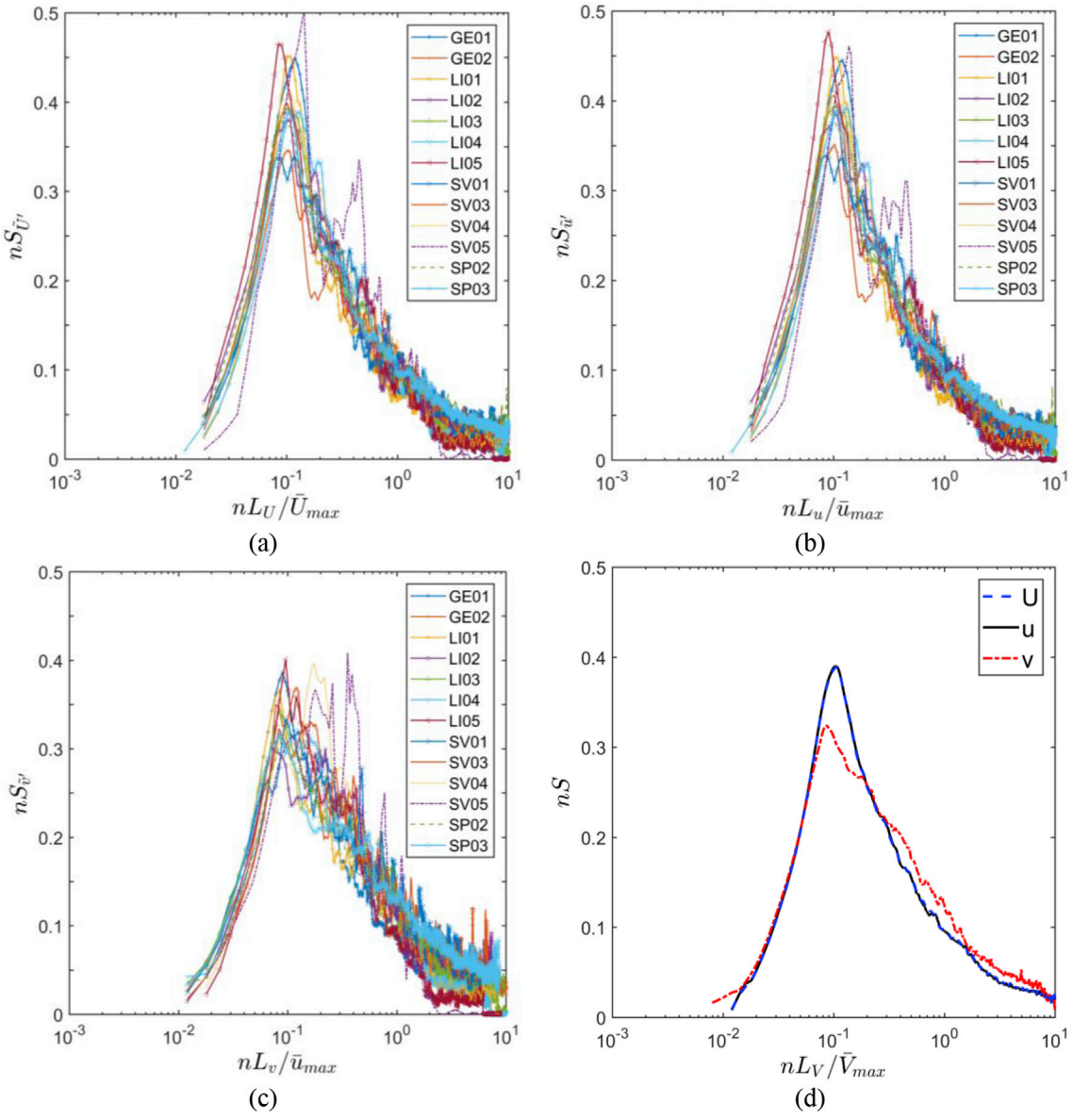

Fig. 23. Ensemble mean values of the PSD of $\tilde{U}'$ (a), $\tilde{u}'$ (b), and $\tilde{v}'$ (c) for every anemometer; mean value of PSD of $\tilde{U}'$, $\tilde{u}'$ and $\tilde{v}'$ for all the records (d), being $V = U,u,v$.

Table 8
Ensemble Mean and Std values of the mean, standard deviation, skewness and kurtosis (m, σ, γ κ) of $\mu_U(t)\tilde{U}'(t)$, $\mu_u(t)\tilde{u}'(t)$ and $\mu_v(t)\tilde{v}'(t)$.

	Parameter	m	σ	γ	κ
$\mu_U\tilde{U}'$	Mean	−0.013	1.082	−0.098	4.380
	Std	0.031	0.041	0.331	1.939
$\mu_u\tilde{u}'$	Mean	0.006	1.086	−0.119	4.376
	Std	0.038	0.045	0.337	1.194
$\mu_v\tilde{v}'$	Mean	0.000	1.085	0.006	4.802
	Std	0.023	0.048	0.325	1.886

explicitly into account the wind direction and decouples the turbulent fluctuations into longitudinal and lateral components. On the contrary, likewise for the methods classically applied to thunderstorm outflows, but diversely from the tradition in synoptic winds, this rule extract the mean wind velocity through a running-mean operator with a moving average period (here $T = 30$ s) shorter than the full length of the record (here $\Delta T = 10$ min). Nevertheless, assuming $T = \Delta T$, the slowly-varying time-histories extracted by this procedure (i.e. the mean wind velocity, the standard deviation and the turbulence intensity) identify themselves with the constant values classically used for synoptic wind speeds. Under these viewpoints the new decomposition rule applies to both synoptic winds and thunderstorm outflows, contains the classical decomposition rule for synoptic winds as a particular case, provides a substantial generalisation of the decomposition rule classically applied to thunderstorm outflows.

A dominant property of the new decomposition rule is that it neither cancels nor distorts the knowledge acquired so far with regard to thunderstorms outflows, but extends the information relating thereto. More precisely, this paper proves that the properties classically extracted from thunderstorm outflows with reference to the resultant wind speed – namely the slowly varying mean wind velocity, the turbulence intensity and its modulation, the reduced turbulent fluctuations, the integral length scales and the power spectral density, and the gust factor - are very close to the ones obtained through the new rule with reference to the

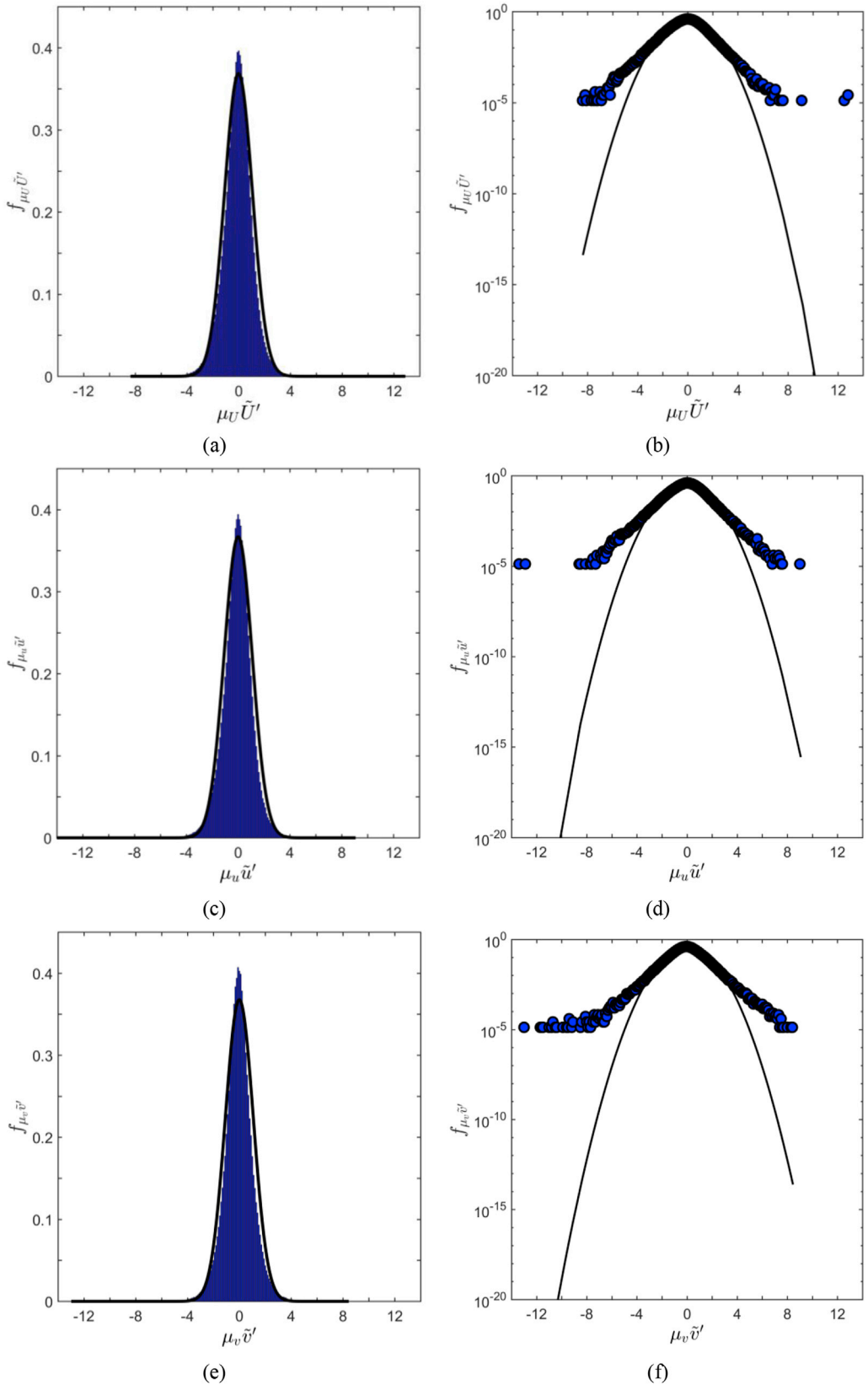

Fig. 24. PDF of $\mu_U(t)\tilde{U}'(t)$, $\mu_u(t)\tilde{u}'(t)$ and $\mu_v(t)\tilde{v}'(t)$: decimal (a) (c) (e) and logarithmic (b) (d) (f) ordinate.

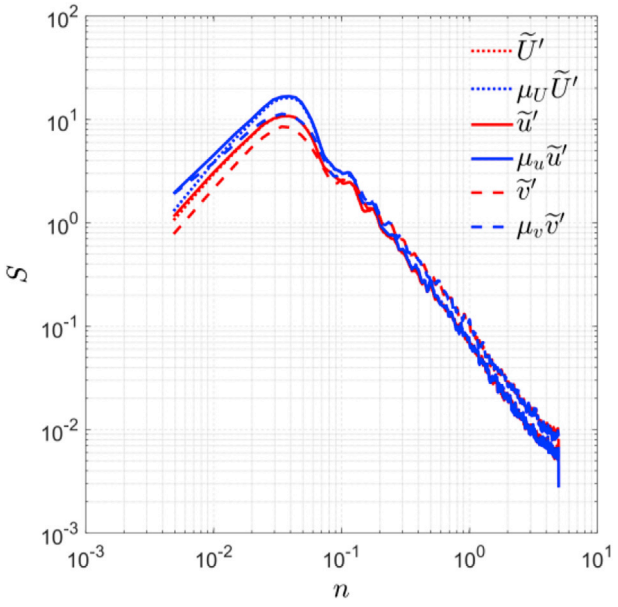

Fig. 25. Ensemble PSD of $\widetilde{U}'$, $\mu_U\widetilde{U}'$, $\widetilde{u}'$, $\mu_u\widetilde{u}'$, $\widetilde{v}'$ and $\mu_v\widetilde{v}'$.

Table 9
Ensemble mean and cov values of the gust factors.

Port	Anem. No.	G_U	Cov(G_U)	G_u	Cov(G_u)
Genoa	1	1.20	0.09	1.21	0.10
	2	1.26	0.08	1.26	0.08
Livorno	1	1.16	0.08	1.16	0.08
	2	1.26	0.09	1.27	0.09
	3	1.16	0.06	1.16	0.06
	4	1.15	0.06	1.15	0.06
	5	1.14	0.02	1.14	0.02
Savona	1	1.24	0.06	1.25	0.06
	2	1.49	0.00	1.50	0.00
	3	1.22	0.06	1.23	0.06
	4	1.25	0.06	1.25	0.06
	5	1.45	0.14	1.47	0.15
La Spezia	2	1.33	0.07	1.34	0.08
	3	1.26	0.08	1.28	0.08
All ports		1.22	0.09	1.23	0.09

longitudinal component of the wind speed. On the other hand the new rule furnishes a thorough information, usually disregarded when adopting the classical decomposition rule, with reference to the slowly-varying mean wind direction and the lateral turbulence component.

It is very worth noting that the properties of the lateral turbulence component of the thunderstorm outflows - i.e. its turbulence intensity and its modulation, the reduced turbulent fluctuations, the integral length scale and the power spectral density - are very similar to the analogous quantities that characterize the longitudinal turbulence component and, for the transitive property, to those that characterize the turbulence classically analysed without decoupling its components. Also, the longitudinal and lateral turbulence components are nearly uncorrelated. These properties derive from the use of a mobile mean wind speed with an averaging period $T = 30$ s: it transfers the low frequency harmonic content to the slowly-varying mean wind velocity and limits the high-frequency harmonic content, indicatively, to the inertial sub-range, where turbulence is locally isotropic or quasi-isotropic.

The novel directional decomposition rule of the wind speed discloses several research prospects in many different fields. First, it creates a common background to model and to analyse the wind speed of both synoptic events and thunderstorm outflows. It represents a fundamental step forward towards implementing thunderstorm models adhering to the reality of these complex phenomena. A clear evaluation of the direction shift of the thunderstorm outflows is fundamental to recognize the travelling nature of the downbursts, to reconstruct their evolution and to clarify the crucial role of the intensification of the wind speed due to the translation of the thunderstorm cell. The decoupling of the longitudinal and lateral turbulence components also for thunderstorm outflows is crucial to inspect the dynamic behaviour of structures in terms of alongwind and crosswind response. The explicit extraction of the slowly-varying mean wind direction opens the doors to take into account the evolution of the angle of attack of the wind speed in the course of transient wind events; this may be crucial for problems dominated by aerodynamic and aeroelastic features.

Independently of these research prospects concerning the novel decomposition rule, authors wish to point out three key issues that go beyond this specific topic: 1) the interaction between the downburst and the background flow, and the possibility of separating their effects; 2) the role of the terrain roughness, especially close to the ground; and, 3) the shape of the slowly-varying mean wind velocity profile and direction, with special regard to its evolution on time. Several tasks of the

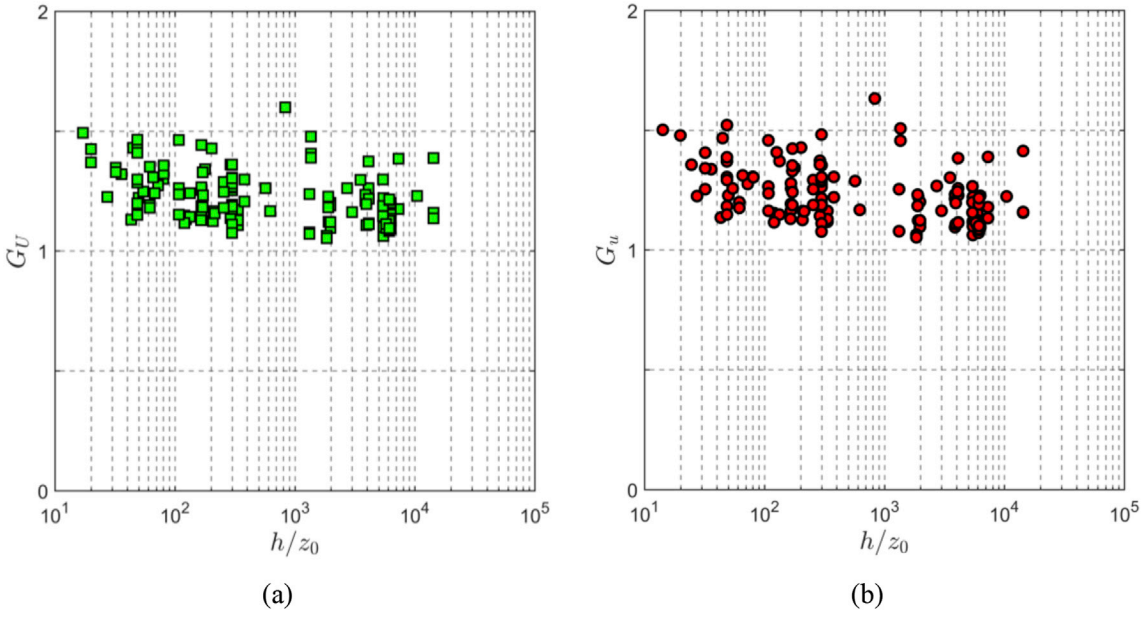

Fig. 26. Gust factor as a function of h/z_0: (a) G_U; (b) G_u.

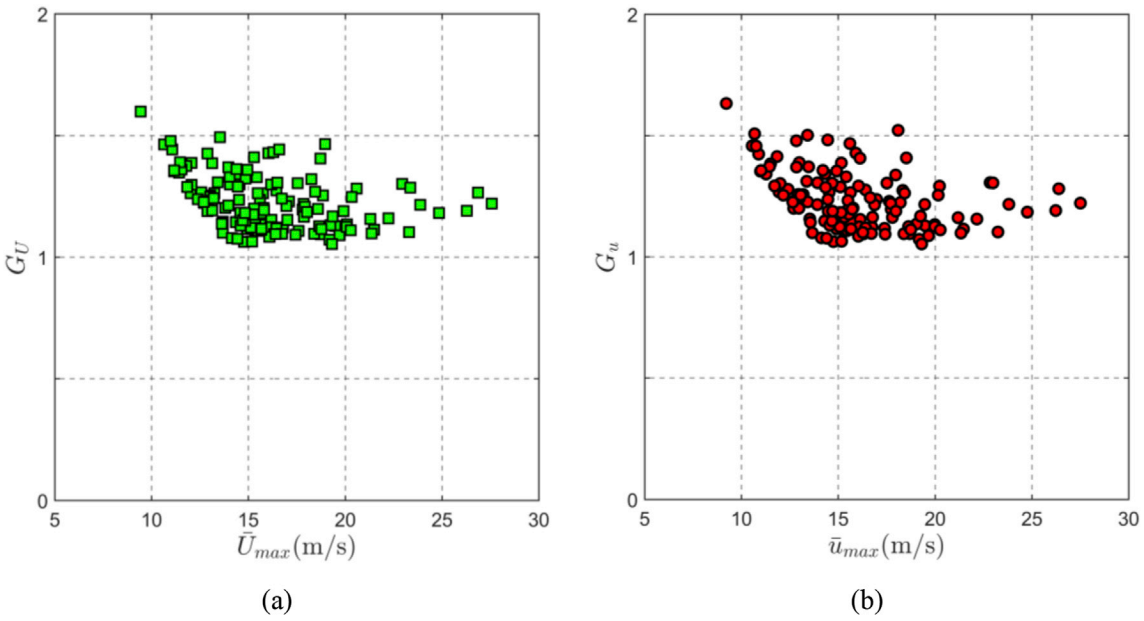

Fig. 27. Gust factor as a function of the maximum value of the slowly-varying mean wind velocity: (a) G_U; (b) G_u.

THUNDERR Project are aimed at clarifying these aspects. The new decomposition rule proposed herein is a robust and helpful tool to pursue these objectives.

Acknowledgements

This research is funded by European Research Council under the European Union's Horizon 2020 research and innovation program (grant agreement No. 741273) for the project THUNDERR - Detection, simulation, modelling and loading of thunderstorm outflows to design wind safer and cost-efficient structures – through an Advanced Grant 2016. This work is also supported by the National Natural Science Foundation of China (51720105005) and 111 Project of China (B18062, B13002). The data used for this research were recorded by the monitoring network set up as part of the European Projects “Winds and Ports” (grant No. B87E09000000007) and “Wind, Ports and Sea” (grant No. B82F13000100005), funded by the European Territorial Cooperation Objective, Cross-border program Italy-France Maritime 2007–2013.

References

Abd-Elaal, E.S., Mills, J.E., Ma, X., 2013. A coupled parametric-CFD study for determining ages of downbursts through investigation of different field parameters. J. Wind Eng. Ind. Aerod. 123, 30–42.
Asano, K., Iida, Y., Uematsu, Y., 2019. A laboratory study of wind loads on a low-rise building in a downburst using a moving pulsed jet simulator and their comparison with other types of simulators. J. Wind Eng. Ind. Aerod. 184, 313–320.
Burlando, M., De Gaetano, P., Pizzo, M., Repetto, M.P., Solari, G., Tizzi, M., 2013. Wind climate analysis in complex terrain. J. Wind Eng. Ind. Aerod. 123, 349–362.
Burlando, M., Romanic, D., Solari, G., Hangan, H., Zhang, S., 2017. Field data analysis and weather scenario of a downburst event in Livorno, Italy on 1 October 2012. Mon. Weather Rev. 145, 3507–3527.
Burlando, M., Zhang, S., Solari, G., 2018. Monitoring, cataloguing and weather scenarios of thunderstorm outflows in the Northern Mediterranean. Nat. Hazards Earth Syst. Sci. 18, 2309–2330.
Castino, F., Rusca, L., Solari, G., 2003. Wind climate micro-zoning: a pilot application to Liguria Region (North-Western Italy). J. Wind Eng. Ind. Aerod. 91, 1353–1375.
Chay, M.T., Albermani, F., Wilson, B., 2006. Numerical and analytical simulation of downburst wind loads. Eng. Struct. 28, 240–254.
Chen, X., 2008. Analysis of alongwind tall building response to transient nonstationary winds. J. Struct. Eng. ASCE 134, 782–791.
Chen, L., Letchford, C.W., 2004a. A deterministic-stochastic hybrid model of downbursts and its impact on a cantilevered structure. Eng. Struct. 26, 619–629.
Chen, L., Letchford, C.W., 2004b. Parametric study on the alongwind response of the CAARC building to downbursts in the time domain. J. Wind Eng. Ind. Aerod. 92, 703–724.
Chen, L., Letchford, C.W., 2005. Proper orthogonal decomposition of two vertical profiles of full-scale nonstationary downburst wind speeds. J. Wind Eng. Ind. Aerod. 93, 187–216.
Chen, L., Letchford, C.W., 2006. Multi-scale correlation analyses of two lateral profiles of full-scale downburst wind speeds. J. Wind Eng. Ind. Aerod. 94, 675–696.
Chen, L., Letchford, C.W., 2007. Numerical simulation of extreme winds from thunderstorm downbursts. J. Wind Eng. Ind. Aerod. 95, 977–990.
Choi, E.C.C., 2000. Wind characteristics of tropical thunderstorms. J. Wind Eng. Ind. Aerod. 84, 215–226.
Choi, E.C.C., Hidayat, F.A., 2002. Dynamic response of structures to thunderstorm winds. Prog. Struct. Eng. Mater. 4, 408–416.
Davenport, A.G., 1961. The application of statistical concepts to the wind loading of structures. Proc. Inst. Civ. Eng. 19, 449–472.
De Gaetano, P., Repetto, M.P., Repetto, T., Solari, G., 2014. Separation and classification of extreme wind events from anemometric records. J. Wind Eng. Ind. Aerod. 126, 132–143.
Engineering Sciences Data Unit, 1993. Computer Program for Wind Speeds and Turbulence Properties: Flat or Hill Sites in Terrain with Roughness Changes. ESDU Item 92032, London, UK.
Flay, R.G.J., Stevenson, D.C., 1988. Integral length scales in strong winds below 20 m. J. Wind Eng. Ind. Aerod. 28, 21–30.
Fujita, T.T., 1985. Downburst: Microburst and Macroburst. University of Chicago Press, Chicago, IL.
Gomes, L., Vickery, B.J., 1977/1978. Extreme wind speeds in mixed climates. J. Ind. Aerodyn. 2, 331–344.
Hjelmfelt, M.R., 1988. Structure and life cycle of microburst outflows observed in Colorado. J. Appl. Meteorol. 27, 900–927.
Holmes, J.D., Hangan, H.M., Schroeder, J.L., Letchford, C.W., Orwig, K.D., 2008. A forensic study of the Lubbock-Reese downdraft of 2002. Wind Struct. 11, 19–39.
Holmes, J.D., Oliver, S.E., 2000. An empirical model of a downburst. J. Ind. Aerodyn. 22, 1167–1172.
Huang, G., Chen, X., Liao, H., Li, M., 2013. Predicting tall building response to nonstationary winds using multiple wind speed samples. Wind Struct. 17 (2), 227–244.
Huang, G., Zheng, H., Xu, Y., Li, Y., 2015. Spectrum models for nonstationary extreme winds. J. Struct. Eng. 141 (10), 04015010.
Ivan, M., 1986. A ring-vortex downburst model for flight simulations. J. Aircr. 23, 232–236.
Kasperski, M., 2002. A new wind zone map of Germany. J. Wind Eng. Ind. Aerod. 90, 1271–1287.
Kwon, D.K., Kareem, A., 2009. Gust-front factor: new framework for wind load effects on structures. J. Struct. Eng. ASCE 135, 717–732.
Letchford, C.W., Mans, C., Chay, M.T., 2002. Thunderstorms – their importance in wind engineering (a case for the next generation wind tunnel). J. Wind Eng. Ind. Aerod. 90, 1415–1433.
Lombardo, F.T., Main, J.A., Simiu, E., 2009. Automated extraction and classification of thunderstorm and non-thunderstorm wind data for extreme-value analysis. J. Wind Eng. Ind. Aerod. 97, 120–131.
Lombardo, F.T., Smith, D.A., Schroeder, J.L., Mehta, K.C., 2014. Thunderstorm characteristics of importance to wind engineering. J. Wind Eng. Ind. Aerod. 125, 121–132.
McCullough, M., Kwon, D.K., Kareem, A., Wang, L., 2014. Efficacy of averaging interval for nonstationary winds. J. Eng. Mech. ASCE 140, 1–19.

Miguel, L.F.F., Riera, J.D., Miguel, L.F.F., 2018. Assessment of downburst wind loading on tall structures. J. Wind Eng. Ind. Aerod. 174, 252–259.
Orwig, K.D., Schroeder, J.L., 2007. Near-surface wind characteristics of extreme thunderstorm outflows. J. Wind Eng. Ind. Aerod. 95, 565–584.
Oseguera, R.M., Bowles, R.L., 1988. A simple analytic 3-dimensional downburst model based on boundary layer stagnation flow. NASA Tech. Memo. 100632.
Piccardo, G., Solari, G., 2000. 3-D wind-excited response of slender structures: closed form solution. J. Struct. Eng. ASCE 126, 936–943.
Ponte Jr., J., Riera, J.D., 2007. Wind velocity field during thunderstorms. Wind Struct. 10, 287–300.
Ponte Jr., J., Riera, J.D., 2010. Simulation of extreme wind series caused by thunderstorms in temperate latitudes. Struct. Saf. 32, 231–237.
Peng, L., Huang, G., Chen, X., Yang, Q., 2018. Evolutionary spectra-based time-varying coherence function and application in structural response analysis to downburst winds. J. Struct. Eng. ASCE 144 (7), 04018078.
Repetto, M.P., Burlando, M., Solari, G., De Gaetano, P., Pizzo, M., Tizzi, M., 2018. A web-based GIS platform for the safe management and risk assessment of complex structural and infrastructural systems exposed to wind. Adv. Eng. Software 117, 29–45.
Riera, J.D., Ponte Jr., J., 2012. Recent Brazilian research on thunderstorm winds and their effects on structural design. Wind Struct. 15, 111–129.
Romanic, D., Lo Tufo, J., Hangan, H., 2019. Transient behavior in impinging jets in crossflow with application to downburst flows. J. Wind Eng. Ind. Aerod. 184, 209–227.
Schultz, T.A., 1990. Multiple vortex ring model of the DFW microburst. J. Aircr. 27, 163–168.
Solari, G., 2014. Emerging issues and new frameworks for wind loading on structures in mixed climates. Wind Struct. 19, 295–320.
Solari, G., 2016. Thunderstorm response spectrum technique: theory and applications. Eng. Struct. 108, 28–46.
Solari, G., Burlando, M., De Gaetano, P., Repetto, M.P., 2015a. Characteristics of thunderstorms relevant to the wind loading of structures. Wind Struct. 20, 763–791.
Solari, G., De Gaetano, P., Repetto, M.P., 2015b. Thunderstorm response spectrum: fundamentals and case study. J. Wind Eng. Ind. Aerod. 143, 62–77.
Solari, G., Piccardo, G., 2001. Probabilistic 3-D turbulence modeling for gust buffeting of structures. Probabilist. Eng. Mech. 16, 73–86.
Solari, G., Repetto, M.P., Burlando, M., De Gaetano, P., Pizzo, M., Tizzi, M., Parodi, M., 2012. The wind forecast for safety and management of port areas. J. Wind Eng. Ind. Aerod. 104, 266–277.
Solari, G., Rainisio, D., De Gaetano, P., 2017. Hybrid simulation of thunderstorm outflows and wind-excited response of structures. Meccanica 52, 3197–3220.
Solari, G., De Gaetano, P., 2018. Dynamic response of structures to thunderstorm outflows: response spectrum technique vs time-domain analysis. Eng. Struct. 176, 188–207.
Su, Y., Huang, G., Xu, Y., 2015. Derivation of time-varying mean for non-stationary downburst winds. J. Wind Eng. Ind. Aerod. 141, 39–48.
Van der Hoven, I., 1957. Power spectrum of horizontal wind speed in the frequency range from 0.0007 to 900 cycles per hour. J. Meteorol. 14, 160–164.
Vicroy, D.D., 1991. A simple, analytical, axisimmetric microbust model for downdraft estimation. NASA Tech. Memo. 104053.
Vicroy, D.D., 1992. Assessment of micro-burst models for downdraft estimation. J. Aircr. 29, 1043–1048.
Xu, Z., Hangan, H., 2008. Scale, boundary and inlet condition effects on impinging jets. J. Wind Eng. Ind. Aerod. 96, 2383–2402.
Zhang, S., Solari, G., De Gaetano, P., Burlando, M., Repetto, M.P., 2018a. A refined analysis of thunderstorm outflow characteristics relevant to the wind loading of structures. Probabilist. Eng. Mech. 54, 9–24.
Zhang, S., Solari, G., Yang, Q.S., Repetto, M.P., 2018b. Extreme wind speed distribution in a mixed wind climate. J. Wind Eng. Ind. Aerod. 176, 239–253.
Zhu, S., Etkin, B., 1985. Model of the wind field in a downburst. J. Aircr. 22, 595–601.